UNIVERSIDAD NACIONAL AUTÓNOMA DE MÉXICO
PROGRAMA DE MAESTRÍA Y DOCTORADO EN INGENIERÍA
INGENIERÍA ELÉCTRICA - CONTROL

FAST EXTREMUM SEEKING FOR BIOREACTORS USING A VARIABLE STRUCTURE CONTROL APPROACH

TESIS
QUE PARA OPTAR POR EL GRADO DE:
MAESTRO EN INGENIERÍA ELÉCTRICA

PRESENTA:
ULISES RAMÍREZ CARMONA

TUTORES:
DR. JAIME ALBERTO MORENO PÉREZ
INSTITUTO DE INGENIERÍA
DR. ALEJANDRO VARGAS CASILLAS
INSTITUTO DE INGENIERÍA

CIUDAD DE MÉXICO, AGOSTO 2018

Universidad Nacional Autónoma de México
UNAM
Biblioteca Central
Dirección General de Bibliotecas de la UNAM

UNAM – Dirección General de Bibliotecas
Tesis Digitales
Restricciones de uso

DERECHOS RESERVADOS ©
PROHIBIDA SU REPRODUCCIÓN TOTAL O PARCIAL

Todo el material contenido en esta tesis esta protegido por la Ley Federal del Derecho de Autor (LFDA) de los Estados Unidos Mexicanos (México).

El uso de imágenes, fragmentos de videos, y demás material que sea objeto de protección de los derechos de autor, será exclusivamente para fines educativos e informativos y deberá citar la fuente donde la obtuvo mencionando el autor o autores. Cualquier uso distinto como el lucro, reproducción, edición o modificación, será perseguido y sancionado por el respectivo titular de los Derechos de Autor.

JURADO ASIGNADO:

Presidente:	Dr. Jesús Alvarez Calderón
Secretario:	Dr. Edmundo Gabriel Rocha Cózatl
Vocal:	Dr. Jaime Alberto Moreno Pérez
1er. Suplente:	Dr. Alejandro Vargas Casillas
2o. Suplente:	Dr. Leonid Fridman

La tesis se realizó en el Instituto de Ingeniería, UNAM.

TUTOR DE TESIS:

Dr. Jaime Alberto Moreno Pérez
Instituto de Ingeniería

_____

Dedicado con mucho cariño a mis padres y a todas las personas
que me han brindado su apoyo y afecto incondicionalmente
a lo largo de mi vida, por mostrarme que todavía
existen personas valiosas en este mundo.

Agradecimientos

En primer lugar agradezco a todos los miembros de mi familia, tanto biológica como adoptiva porque su apoyo fue esencial para culminar mis estudios.

A mis amigos, por ser una fuente interminable de alegrías y experiencias; por estar a mi lado durante el proceso y en todo momento; por todas las horas en que charlamos, disfrutamos de la vida y por todo lo que he aprendido de ustedes.

A mi novia quien, a pesar de haber llegado inesperadamente a mi vida, es una fuente muy grande de inspiración que me motiva a ser mejor cada día. Llegó en la última etapa de la realización del presente escrito, pero me impulsó en todo momento para terminarlo.

A mis asesores de tesis, los doctores Jaime A. Moreno Pérez y Alejandro Vargas, quienes me guiaron en todo el proceso y me ayudaron a sortear las dificultades técnicas del trabajo.

A los compañeros del Seminario de Modos Deslizantes, quienes contribuyeron en la mejora continua de mi trabajo con sus observaciones y críticas constructivas, y en especial a Gustavo Rueda, quien siempre tuvo la disposición de revisar los avances de mi tesis y proporcionarme realimentación valiosa.

A los miembros del jurado, por el tiempo destinado a la lectura del manuscrito original, y sus valiosos comentarios que ayudaron a enriquecer el presente trabajo.

Finalmente, agradezco al CONACYT por el apoyo económico brindado para la realización de mis estudios de maestría.

Contents

List of Figures

Chapter 1

Introduction

1.1 Motivation

In a wastewater treatment plant, besides obtaining clean water, other useful resources may be recovered. Biogas is one of the resources that can be produced, which is extremely useful because it is flammable and an important energy vector, containing a significant amount of methane or other combustible gases.

The most common process for converting liquid waste into biogas is anaerobic digestion, where microorganisms degrade the organic matter and convert some of them into biogas, composed mainly of methane (CH_4) and carbon dioxide (CO_2). The waste feed stream may be high strength wastewater, excess sludge from wastewater treatment, or the organic fraction of municipal solid waste, among others Batstone (2006). The amount of biogas produced depends on several factors, including the influent composition and concentrations, the feed rate, the reaction rate as well as the parameters of the process, which are usually highly uncertain and difficult to determine. However, a usual objective is to produce as much biogas as possible despite these uncertainties/perturbations.

1.2 Objective

The objective of this work is to design an extremum seeking controller for maximizing biogas production of a second order bioreactor model, which provides robustness against uncertainty in parameters and noise in measurements, independent of the reaction rate. Also, it is necessary that this technique guarantees faster convergence than traditional ones by measuring only the output.

1.3 Problem statement

We consider a (typical) simplified model for a bioreactor Andrews (1968), Antonelli and Astolfi (2000), which has two states: a biomass (concentration) $x \in \mathbb{R}_{\geq 0}$ and a substrate (concentration) $s \in \mathbb{R}_{\geq 0}$. The x variable models a population of microorganisms which is fed with substrate s_{in} (inlet substrate) with a rate u (dilution rate). The biomass degrades the substrate with a certain growth function $\mu(s)$ (reaction rate), and also it is produced an amount of biogas Q.

In some reactors, there is a matrix in which biomass is retained (for biohydrogen production it is made by loofah sponge, expanded clay or activated carbon Chang et al. (2002), it is considered a biomass retention parameter $\alpha \in (0, 1]$ modelling that phenomenon. When $\alpha = 1$ there is no biomass retention and a Continuous Stirred Tank Reactor (CSTR), and for $\alpha = 0$ all biomass is retained and this corresponds to a Fixed-Bed Reactor (FBR). In Figure 1.1, it is shown a Partially Fixed-Bed Reactor (PFBR), i.e., $\alpha \in (0, 1)$; the central tube represents the matrix that supports a fraction of the internal bacteria.

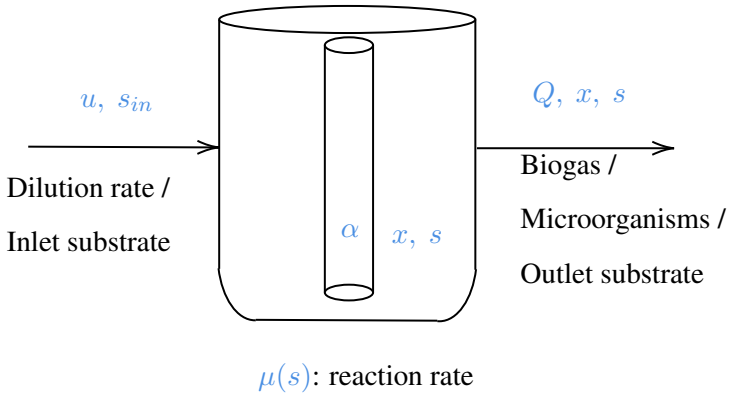

Figure 1.1: Partially Fixed-Bed Reactor

The simplified bioreactor dynamics is described by the mass balance equations

$$\begin{aligned} \dot{x} &= (-\alpha u + \mu(s))x, \\ \dot{s} &= -d\mu(s)x + u(s_{in} - s), \\ Q &= q\mu(s)x, \end{aligned} \tag{1.1}$$

where: $u \in \mathbb{R}_{\geq 0}$ is the dilution rate (input), $\mu \in \mathbb{R}_{\geq 0}$ is a continuous differentiable function representing the reaction rate (it is assumed that $\mu(0) = 0$), $d \in \mathbb{R}_{\geq 0}$ is the constant yield coefficient, s_{in} is the (here assumed constant) substrate concentration in the input flow of the bioreactor, $q \in \mathbb{R}_{\geq 0}$ is a constant conversion factor and $Q \in \mathbb{R}_{\geq 0}$ is the flow rate of gas produced in the bioreactor, which is assumed as the only measured variable.

The operation of the bioreactor with constant values of input u is usual, and different equilibrium points are obtained for each u. Since the production of biogas is of interest in our application, we want to operate the bioreactor at the equilibrium point for which Q is maximized, i.e., the production of biogas is maximal among all possible equilibrium points. Assumption 1 is a necessary and sufficient condition for the existence of one and only one optimal operating point, which is necessary to have a well-defined problem. It will be justified analytically in the next chapter. (In Fed-Batch culture, the optimal condition is achieved when $s = s_c$ Lara-Cisneros et al. (2014), i.e., maximizing the reaction rate $\mu(s)$. However, in continuous culture the optimal condition is obtained with a smaller value of inlet substrate.)

Assumption 1. *The reaction rate $\mu(s)$ is such that*

$$\frac{\mathrm{d}\mu(\bar{s})}{\mathrm{d}\bar{s}}(s_{in} - \bar{s}) - \mu(\bar{s}) = 0,$$

has one and only one solution s^* in the compact $\bar{s} \in [0, s_{in}]$.

Reaction rate models satisfying assumption 1 are very common, i.e., typical reaction rates which satisfy it are:

1. Monod model: this is a monotone growing function given by the expression

$$\mu(s) = \frac{\mu_0 s}{K_s + s}, \tag{1.2}$$

whose behavior can be appreciated in Figure 1.2.

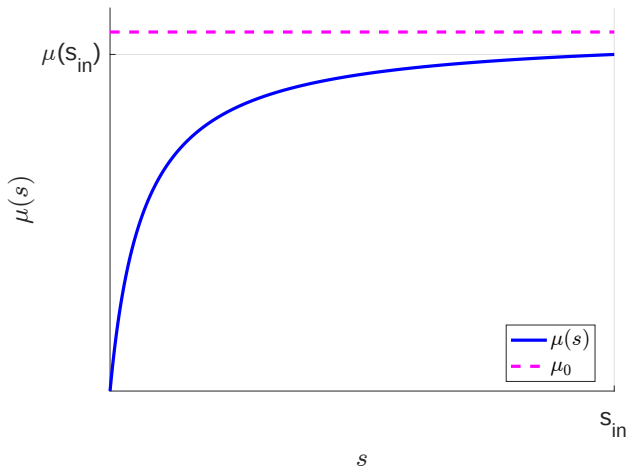

Figure 1.2: Monod reaction rate.

2. Haldane model: this corresponds to an inhibitory substrate and it is usually decribed by the expression

$$\mu(s) = \frac{\mu_0 s}{K_s + s + \frac{s^2}{K_I}}, \tag{1.3}$$

whose behavior is shown in Figure 1.3 ($s_c = \sqrt{K_s K_I}$, $\mu(s_c) < \mu_0$). Without loss of generality, it is supposed that $s_{in} > s_c$ for eliminating the monotonous case.

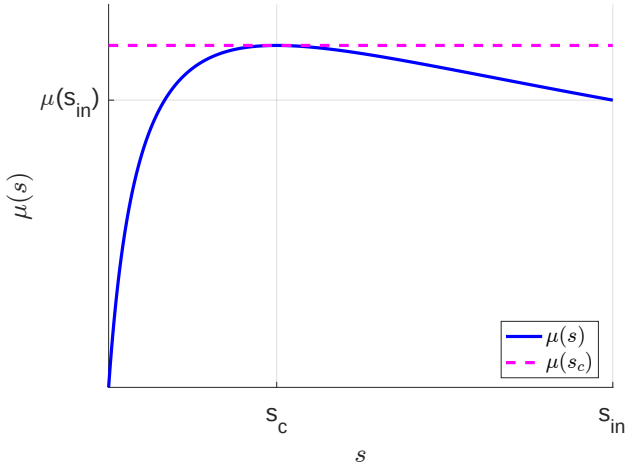

Figure 1.3: Haldane reaction rate.

Our problem consists in designing a controller that drives system trajectories to the optimal operating point (the operating point in which Q is maximized). Also, the controller has to satisfy the following conditions:

- The only measurable variable is the output, which has to be defined depending on the value of α.
- It has to be independent of the reaction rate $\mu(s)$ (satisfying Assumption 1).
- It has to be robust against uncertainty on parameters.
- It has to be a saturated.

1.4 State of the art

The optimization of this system (when $\alpha = 1$) has been studied for several decades. There are many ways to achieve this objective such as the regulation of the optimal operating point or extremum seeking (ES) techniques. Here are presented examples, and the assumptions that were made in each approach.

One (natural) strategy to reach this objective is to calculate the value of (for example) x at the equilibrium which maximizes Q (Q_{max}) and to regulate it at this value. For instance, Schaum et al. (2012) developed a saturated output feedback controller to regulate the optimal operating point considering a Haldane reaction rate. However, it requires the measurement of x and the knowledge of the model and its parameters in a precise manner.

Another way to avoid this is using some kind of ES strategy. Wang et al. (1999) designed an ES technique that requires to know the particular form of the reaction rate, i.e., whether it is Monod or Haldane. Their main drawback occurs in the Haldane case because it is necessary a state feedback for stabilizing the optimal operating point. For Monod reaction rate, ES requires only the measurement of the output, but it has the disadvantage that the objective is reached very slowly, since ES requires to operate near quasi-stationary states.

Other example is the adaptive ES controller proposed by Marcos et al. (2004), where it was designed an adaptive algorithm for estimating system parameters, but it has the disadvantage that only works for Haldane kinetics. Additionally, it was assumed that s and Q are measured, which is a stronger condition than traditional ones of ES.

By using a Neural Networks approach, Guay et al. (2004) designed an ES controller that works for bounded continuous reaction rates, i.e., not only for Monod or Haldane kinetics. However, it is supposed that both states (x and s) are measurable.

Dieulot (2012) presented an output feedback controller that is independent on the reaction rate, but it has some problems to avoid the washout state in the Haldane case. In that paper, they assumed that x and $P = ux$ are measured.

A variable structure controller for a bioreactor in fed-batch culture was presented by Lara-Cisneros et al. (2014), which is related to the time-optimal control proposed by Moreno (1999). Nevertheless, it is very different to the one presented here because it uses equivalent control Sira-Ramírez (1988) in combination with a high gain observer. Also, it requires the measurements of Q and s, and a non-monotonic kinetics which is very restrictive as the Monod case is excluded.

The objective of this work is to propose a different strategy to cope with all these problems. It could be called a *fast extremum seeking* (FES) strategy, since it is able to reach the objective faster than with traditional ES, i.e., with a closed-loop settling time similar to the open-loop settling time (when is applied the constant u that maximizes biogas production).

The basic idea is to switch between two constant values of the input variable u whenever the transient maximum value of the output is reached, and this (surprisingly) leads to attain and keep for all future times the (stationary) optimal value Q_{max}. The controller has some switching surfaces, but there is also a rather atypical sliding set, since it is a manifold of the same

dimension of the state space (and not, as usually happens of lower dimension). The controller switches with high frequency on this manifold.

1.5 Contributions

- The analysis of a second order bioreactor model was made, considering a biomass retention parameter. It was found a positive-invariant set for constant inputs ($u \in [0, \infty)$).
- An ES controller for optimizing biogas production in a second order bioreactor model was designed, achieving the optimal-operating-point considering an unknown reaction rate and unknown constant parameters. The output being available for measurement is the only requirement.
- The closed-loop turned out faster than provided by traditional ES, additionally the proposed algorithm showed robustness against noise in measurements and time-varying inlet substrate.

1.6 Outline of the thesis

This work is divided in five chapters. After this introduction and problem formulation, Chapter Two analyses the second order bioreactor model, i.e., the optimal-operating-point conditions are obtained; system trajectories are analysed in the phase plane; and finally it is found a positive-invariant set for trajectories with constant inputs.

Chapter Three presents the controller design for the Continuous Stirred Tank Reactor (there is no biomass retention). It is important to mention that, in order to give sense to closed-loop solutions, *sample-and-hold* solutions are introduced. The controller is tested both in ideal and realistic scenarios showing a very good performance.

Chapter Four extends previous results to Partially Fixed-Bed Reactors by introducing a new output. The controller is also tested in different scenarios, once again, with excellent results.

Finally, Chapter Five presents the conclusions of this work and some guidelines for future research.

Chapter 2

System Analysis

2.1 Equilibrium (operating) points

For calculating the equilibrium of (1.1), the following algebraic equations must be solved

$$\begin{aligned} 0 &= (-\alpha\bar{u} + \mu(\bar{s})\bar{x}, \\ 0 &= -d\mu(\bar{s})\bar{x} + \bar{u}(s_{in} - \bar{s}), \\ \bar{Q} &= q\mu(\bar{s})\bar{x}, \end{aligned} \tag{2.1}$$

where $\bar{z}$ indicates the stationary value of the corresponding variable. It follows that there are different possible equilibrium points, depending on the value of $\bar{u}$. However, independent of $\bar{u}$, always exists the *washout* condition. It is important to notice that if $\alpha = 0$, the only equilibrium would be the *washout*, therefore it justifies that $\alpha \in (0, 1]$

1. If $\bar{u} = 0$, then the set of equilibria is given by $\bar{s} = 0$ and $\bar{x}$ any positive value. Since there is no biogas production at this steady state, it corresponds to an undesirable operation mode. Another possible equilibrium point corresponds to the washout, i.e. $\bar{x} = 0$ and $\bar{s} \geq 0$. However, this cannot be attained using the zero input, unless it is the initial condition.

2. Additionally to the washout, there are other equilibrium points satisfying the following relations:

$$\begin{aligned} \bar{u} &= \frac{\mu(\bar{s})}{\alpha}, \\ \bar{x} &= \frac{s_{in} - \bar{s}}{d\alpha}. \end{aligned} \tag{2.2}$$

   (a) Monod: If $0 < \bar{u} < \frac{\mu(s_{in})}{\alpha}$ there is one equilibrium point.

   (b) Haldane: If $0 < \bar{u} < \frac{\mu(s_{in})}{\alpha}$ there is one equilibrium point, and if $\frac{\mu(s_{in})}{\alpha} \leq \bar{u} < \frac{\mu(s_c)}{\alpha}$) there are two equilibrium points.

3. If $\bar{u} \geq \frac{\mu_{max}}{\alpha} = \frac{\mu(s_{in})}{\alpha}$ (for Monod), or $\bar{u} \geq \frac{\mu_{max}}{\alpha} = \frac{\mu(s_c)}{\alpha}$ (for Haldane), then $\bar{x} = 0$ and $\bar{s} = s_{in}$, which corresponds to the *washout* condition. Note that, from the equation for $\dot{x}$, it follows that when $\bar{u} > \frac{\mu_{max}}{\alpha}$ the washout will be reached, since $\dot{x} = -ax$, with $a > 0 \Rightarrow \lim_{t\to\infty} x(t) = 0$.

2.2 Optimal operating point

If $\bar{u} = 0$ or $\bar{u} \geq \frac{\mu_{max}}{\alpha}$ there is no biogas production. Therefore, if there is an equilibrium in which biogas production is maximized, it must satisfy the operating conditions (2.2).

$$\bar{Q} = q\mu(\bar{s})\bar{x} = q\mu(\bar{s})\frac{s_{in} - \bar{s}}{d\alpha},$$

$$\bar{Q} = \frac{q}{d\alpha}\mu(\bar{s})(s_{in} - \bar{s}).$$

and the maximal value of $\bar{Q}(\bar{s})$ satisfies

$$\frac{\mathrm{d}\bar{Q}}{\mathrm{d}\bar{s}} = \frac{\mathrm{d}}{\mathrm{d}\bar{s}}\left(\frac{q}{d\alpha}\mu(\bar{s})(s_{in} - \bar{s})\right) = 0, \tag{2.3}$$

$$\frac{\mathrm{d}\bar{Q}}{\mathrm{d}\bar{s}} = \frac{q}{d\alpha}\left(\frac{\mathrm{d}\mu(\bar{s})}{\mathrm{d}\bar{s}}(s_{in} - \bar{s}) - \mu(\bar{s})\right) = 0,$$

$$\frac{\mathrm{d}\mu(\bar{s})}{\mathrm{d}\bar{s}}(s_{in} - \bar{s}) - \mu(\bar{s}) = 0. \tag{2.4}$$

If (2.4) has one and only one solution s^* in the compact $\bar{s} \in [0, s_{in}]$, $\bar{Q}(s^*)$ must be a maximum, because $\bar{Q}(0) = \bar{Q}(s_{in}) = 0$ and $\bar{Q} \in \mathbb{R}_{\geq 0}$. Then, define x^*, s^*, u^*, $Q_{max} = \bar{Q}(s^*)$ as the optimal operating values. Notice that the solution to (2.4) is independent of the parameters α, d and q.

2.2.1 Monod reaction rate

Replacing (1.2) in (2.3) and considering $s = \bar{s}$, it is obtained:

$$\frac{\mathrm{d}\bar{Q}}{\mathrm{d}\bar{s}} = \frac{\mathrm{d}}{\mathrm{d}\bar{s}}\left(\frac{q\mu_0}{d\alpha}\frac{s_{in}\bar{s} - \bar{s}^2}{K_s + \bar{s}}\right),$$

$$\frac{\mathrm{d}\bar{Q}}{\mathrm{d}\bar{s}} = \frac{q\mu_0}{d\alpha}\frac{(K_s + \bar{s})(s_{in} - 2\bar{s}) - (s_{in}\bar{s} - \bar{s}^2)}{(K_s + \bar{s})^2} = 0.$$

Previous expressions can be simplified to

$$(K_s + \bar{s})(s_{in} - 2\bar{s}) - (s_{in}\bar{s} - \bar{s}^2) = 0,$$

$$s_{in}K_s - 2K_s\bar{s} + s_{in}\bar{s} - 2\bar{s}^2 - s_{in}\bar{s} + \bar{s}^2 = 0,$$

$$s_{in}K_s - 2K_s\bar{s} - \bar{s}^2 = 0,$$

$$\bar{s}^2 + 2K_s\bar{s} - s_{in}K_s = 0.$$

Obtaining the solution for $\bar{s}$,

$$\bar{s}_{1,2} = -K_s \pm \sqrt{K_s^2 + s_{in}K_s},$$

and due to $\sqrt{K_s^2 + s_{in}K_s} > K_s$, the only positive solution is

$$s^* = -K_s + \sqrt{K_s^2 + s_{in}K_s}, \tag{2.5}$$

which implies that $\bar{Q}(s^*) > 0$, and consequently $Q_{max} = \bar{Q}(s^*)$ is the steady state absolute maximum. The expressions defining the optimal operating conditions are

$$Q_{max} = \frac{q\mu_0}{d\alpha}\frac{s_{in}s^* - s^{*2}}{K_s + s^*} \tag{2.6}$$

$$u^* = \frac{\mu_0}{\alpha}\frac{s^*}{K_s + s^*} = \mu_0\frac{\sqrt{K_s^2 + s_{in}K_s} - K_s}{\sqrt{K_s^2 + s_{in}K_s}} \tag{2.7}$$

2.2.2 Haldane reaction rate

Replacing (1.3) in (2.3) and considering $s = \bar{s}$, it is obtained:

$$\frac{\mathrm{d}\bar{Q}}{\mathrm{d}\bar{s}} = \frac{\mathrm{d}}{\mathrm{d}\bar{s}}\left(\frac{q\mu_0}{d\alpha}\frac{s_{in}\bar{s} - \bar{s}^2}{K_s + \bar{s} + \frac{\bar{s}^2}{K_I}}\right),$$

$$\frac{\mathrm{d}\bar{Q}}{\mathrm{d}\bar{s}} = \frac{q\mu_0}{d\alpha}\frac{(K_s + \bar{s} + \frac{\bar{s}^2}{K_I})(s_{in} - 2\bar{s}) - (s_{in}\bar{s} - \bar{s}^2)(1 + \frac{2}{K_I}\bar{s})}{(K_s + \bar{s} + \frac{\bar{s}^2}{K_I})^2} = 0.$$

Previous expressions can be simplified to

$$\left(K_s + \bar{s} + \frac{\bar{s}^2}{K_I}\right)(s_{in} - 2\bar{s}) - (s_{in}\bar{s} - \bar{s}^2)\left(1 + \frac{2}{K_I}\bar{s}\right) = 0,$$

$$s_{in}K_s - 2K_s\bar{s} + s_{in}\bar{s} - 2\bar{s}^2 + \frac{s_{in}}{K_I}\bar{s}^2 - \frac{2}{K_I}\bar{s}^3 - s_{in}\bar{s} + \bar{s}^2 - \frac{2s_{in}}{K_I}\bar{s}^2 + \frac{2}{K_I}\bar{s}^3 = 0,$$

$$s_{in}K_s - 2K_s\bar{s} - \left(1 + \frac{s_{in}}{K_I}\right)\bar{s}^2 = 0,$$

$$\left(1 + \frac{s_{in}}{K_I}\right)\bar{s}^2 + 2K_s\bar{s} - s_{in}K_s = 0.$$

Obtaining the solution for $\bar{s}$,

$$\bar{s}_{1,2} = \frac{-K_s \pm \sqrt{K_s^2 + \left(1 + \frac{s_{in}}{K_I}\right) s_{in} K_s}}{1 + \frac{s_{in}}{K_I}},$$

and due to $\sqrt{K_s^2 + \left(1 + \frac{s_{in}}{K_I}\right) s_{in} K_s} > K_s$, the only positive solution is

$$s^* = \frac{-K_s + \sqrt{K_s^2 + \left(1 + \frac{s_{in}}{K_I}\right) s_{in} K_s}}{1 + \frac{s_{in}}{K_I}}, \tag{2.8}$$

which implies that $\bar{Q}(s^*) > 0$, and consequently $Q_{max} = \bar{Q}(s^*)$ is the steady state absolute maximum. The expressions defining the optimal operating point are

$$Q_{max} = \frac{q\mu_0}{d\alpha} \frac{s_{in}s^* - s^{*2}}{K_s + s^* + \frac{s^{*2}}{K_I}}, \tag{2.9}$$

$$u^* = \frac{\mu_0}{\alpha} \frac{s^*}{K_s + s^* + \frac{s^{*2}}{K_I}}. \tag{2.10}$$

2.3 Analysis of trajectories with extreme values of u

Consider the systems

$$\Sigma_1 : \begin{cases} \dot{x} = \mu(s)x, \\ \dot{s} = -d\mu(s)x, \end{cases} \tag{2.11}$$

and

$$\Sigma_2 : \begin{cases} \dot{x} = -(\alpha u_H - \mu(s))x, \\ \dot{s} = -d\mu(s)x + u_H(s_{in} - s). \end{cases} \tag{2.12}$$

which were obtained by making $u = u_L = 0$ and $u = u_H > \frac{\mu_{max}}{\alpha}$ in (1.1), respectively (for Monod reaction rate $u_H > \frac{\mu(s_{in})}{\alpha}$ and for Haldane $u_H > \frac{\mu(s_c)}{\alpha}$).

2.3.1 Analysis of Σ_1

Let us introduce the variety of equilibrium points E obtained from (2.2), which is invariant and asymptotically stable (global attractor) for all $u > 0$ when $\alpha = 1$ Schaum et al. (2012).

$$E = \{(x,\, s) \in \mathbb{R}^2_{\geq 0} | s = s_{in} - dx\}. \tag{2.13}$$

Theorem 2. *The locus of trajectories of Σ_1 are parallel lines.*

Proof. In the phase plane, the system dynamics is as follows

$$\frac{\mathrm{d}s}{\mathrm{d}x} = \frac{-d\mu(s)x}{\mu(s)x} = -d,$$

then, by solving the differential equation

$$\int_{s_0}^{s} \frac{\mathrm{d}s}{\mathrm{d}x}\mathrm{d}x = \int_{x_0}^{x} -d\mathrm{d}x,$$

the expression for Σ_1 trajectories is obtained

$$s = -d(x - x_0) + s_0. \tag{2.14}$$

which are parallel lines to E, and therefore if $(x_0, s_0) \in E$ then $(x, s) \in E\ \forall t > 0$. Then, also with $u = 0$, E is a positive invariant set. ■

There is a continuum of equilibrium points at the positive part of x axis, i.e, $\bar{x} \in \mathbb{R}_{\geq 0}$ and $\bar{s} = 0$. Next, it is necessary to prove the stability of the set, and not for a particular point.

Theorem 3. *The set $Z = \{(x, s) \colon x \in \mathbb{R}_{\geq 0}$ and $s = 0\}$ is asymptotically stable for Σ_1 (2.11).*

Proof. Consider the following Lyapunov candidate function

$$V = \frac{1}{2}s^2,$$

which satisfies $V > 0$, $\forall s \neq 0$, and take its time derivative

$$\dot{V} = s\dot{s} = s(-d\mu(s)x) = -d\mu(s)sx,$$

then

$$\dot{V} < 0, \quad x \neq 0,\ s \neq 0.$$

Then s tends to zero, and given that $x \in \mathbb{R}_{\geq 0}$, Z is globally asymptotically stable. ■

2.3.2 Analysis of Σ_2

On the other hand, when u_H is applied, there is only one equilibrium point (the *washout*) which is asymptotically stable, and also it can be shown that it is exponentially stable.

Theorem 4. *For Σ_2 (2.12), the washout ($x = 0$ and $s = s_{in}$) is globally exponentially stable.*

Proof. Consider the following coordinates change

$$\tilde{s} = s - s_{in}, \tag{2.15}$$

then, the transformed system is as follows

$$\begin{aligned} \dot{x} &= -(\alpha u_H - \mu(\tilde{s} + s_{in}))x, \\ \dot{\tilde{s}} &= -d\mu(\tilde{s} + s_{in})x - u_H\tilde{s}. \end{aligned} \tag{2.16}$$

The worst case for $\dot{x}$ occurs if $\mu(s)$ takes its maximum value,

$$\dot{x} \leq -(\alpha u_H - \mu_{max})x,$$

and defining $a = \alpha u_H - \mu_{max} > 0$,

$$\dot{x} \leq -ax, \tag{2.17}$$

which implies that

$$x(t) \leq x_0 e^{-at}. \tag{2.18}$$

Considering that $\mu(s)$ takes its maximum value and $x(t)$ is upper bounded as shown in (2.18), bounds in the solution of $\tilde{s}$ can be obtained by analyzing two cases.

1. The first one is

$$\dot{\tilde{s}}(t) \geq -d\mu_{max}x_0 e^{-at} - u_H\tilde{s}. \tag{2.19}$$

   Solving the differential equation $\dot{\tilde{s}}(t) = -d\mu_{max}x_0 e^{-at} - u_H\tilde{s}$, and from the comparison lemma, it is obtained

$$\tilde{s}(t) \geq -\frac{d\mu_{max}x_0}{u_H - a}e^{-at} + \left(\frac{d\mu_{max}x_0}{u_H - a} + \tilde{s}_0\right)e^{-u_H t}. \tag{2.20}$$

2. The second one is

$$\dot{\tilde{s}}(t) \leq d\mu_{max}x_0 e^{-at} - u_H\tilde{s}. \tag{2.21}$$

   Solving the differential equation $\dot{\tilde{s}}(t) = d\mu_{max}x_0 e^{-at} - u_H\tilde{s}$, and from the comparison lemma, it is obtained

$$\tilde{s}(t) \leq \frac{d\mu_{max}x_0}{u_H - a}e^{-at} - \left(\frac{d\mu_{max}x_0}{u_H - a} - \tilde{s}_0\right)e^{-u_H t}. \tag{2.22}$$

Then, combining the previous results and because $u_H > a$, the solution $\tilde{s}(t)$ is defined for all $t > 0$ and it satisfies

$$|\tilde{s}(t)| \leq \frac{d\mu_{max}x_0}{u_H - a}e^{-at} - \left(\frac{d\mu_{max}x_0}{u_H - a} - |\tilde{s}_0|\right)e^{-u_H t}. \tag{2.23}$$

Finally, from (2.18) and (2.23) it is concluded that $(0, s_{in})$ is globally exponentially stable. ■

2.4 Positive invariant set Ω

In this section a set (subset of $\mathbb{R}^2_{\geq 0}$) for bioreactor trajectories is defined, which is *positive invariant* (if it contains the system state at some time, then it will contain it also in the future Bacciotti (2013)). Previous research about the bioreactor, e.g. Schaum et al. (2012), found invariant sets for (1.1) when $u > 0$ (for $\alpha = 1$). However, our approach considers $u \geq 0$ and the parameter $\alpha \in (0, 1]$, which leads to slightly different admissible trajectories. In some sense, it is an adaptation from the obtained results in Exothermic Continuous Reactors Álvarez and Franco (2016) because the region is a trapezium.

Looking at Theorem 2 and the region proposed by Schaum et al. (2012) we can define the following set Ω, which geometrically is a trapezium (Figure 2.1).

$$\Omega = \left\{(x,\, s) \in \mathbb{R}^2_{\geq 0} \mid\ 0 \leq x \leq \beta(s), 0 \leq s \leq s_{in}\right\}, \tag{2.24}$$

$$\beta(s) = \frac{2s_{in} - \alpha s}{d\alpha}. \tag{2.25}$$

where $\beta(s)$ is a parallel line to E (2.13) which pases through $(x, s) = \left(\frac{2s_{in}}{d\alpha}, 0\right)$.

Theorem 5. *The set* Ω (2.24) *is positive invariant for the system* (1.1) *with constant inputs.*

Proof. It is convenient to recall Nagumo's Theorem which is going to be useful for this proof. This version was extracted from Blanchini (1999).

> **Nagumo's Theorem:** Consider the system $\dot{x} = f(x)$, and assume that, for each initial condition in a set $\mathbb{R}^n$, it admits a globally unique solution. Let $\Omega \subseteq \mathbb{R}^n$ be a closed and convex set. Then, the set Ω is positive invariant for the system if and only if
>
> $$f(x) \in \mathcal{C}_\Omega(x),\ \forall x \in \Omega. \tag{2.26}$$
>
> Where
>
> $$\mathcal{C}_\Omega(x) = \left\{z \in \mathbb{R}^n : \liminf_{h \to 0} \frac{\text{dist}(x + hz, \Omega)}{h} = 0\right\}. \tag{2.27}$$
>
> is the tangent cone to Ω in x and $\text{dist}(x + hz, \Omega)$ depends on the considered norm.

The geometric interpretation of the theorem is also given in Bacciotti (2013). It says that if, for $x \in \partial\Omega$ (boundary of Ω), the derivative $\dot{x}$ *points inside or is tangent to* Ω, then the trajectory remains in Ω. Also, the generalization for $\dot{x} = f(x, u)$ is valid.

Another useful tool is the inner product. The scalar product (or dot product) between two vectors $\vec{a}, \vec{b} \in \mathbb{R}^n$ is denoted by $\vec{a} \cdot \vec{b}$ and is given by

$$\vec{a} \cdot \vec{b} \equiv |\vec{a}||\vec{b}| \cos(\theta) \equiv \sum_{i=1}^{n} a_i b_i, \ 0 \leq \theta \leq \pi, \tag{2.28}$$

where θ is the angle between the two vectors placed *tail to tail* or *head to head*, and a_i and b_i are the components of the vector $\vec{a}$ and $\vec{b}$, respectively. Then, the value of the dot product $\vec{a} \cdot \vec{b}$ equals the magnitude of $\vec{a}$ multiplied by the projection $\vec{b}$ onto $\vec{a}$. Attending to the signum of $(\vec{a} \cdot \vec{b})$, there are two cases which can be considered:

- $\vec{a} \cdot \vec{b} \geq 0 \Rightarrow 0 \leq \theta \leq \frac{\pi}{2}$,
- $\vec{a} \cdot \vec{b} \leq 0 \Rightarrow \frac{\pi}{2} \leq \theta \leq \pi$.

Let

$$\vec{v} = \begin{bmatrix} -(u - \mu(s))x \\ -d\mu(s)x + u(s_{in} - s) \end{bmatrix}, \tag{2.29}$$

where $\vec{v}$ is the system (3.1) in vectorial notation.

To prove the positive invariance of Ω, it is necessary to show that trajectories cannot leave that region by crossing its boundaries. As the trapezium has four sides and four vertexes (Figure 2.1), the analysis is divided in two stages. In the first, the normal vector $\vec{n}$ (outward-pointing) to the analysed boundary is found. After that, the dot product $\vec{n}$ and the vector field $\vec{v}$ (evaluated at the boundary) is taken in order to verify the signum of the projection. The second stage consists in analyzing dynamics in the vertexes, to see that $\dot{x}$ points inside Ω. If for all boundaries the scalar product $\vec{v} \cdot \vec{n}$ is less than or equal to zero, it will be concluded that $\dot{x}$ *points inside or is tangent to* Ω.

1. **Boundaries:**

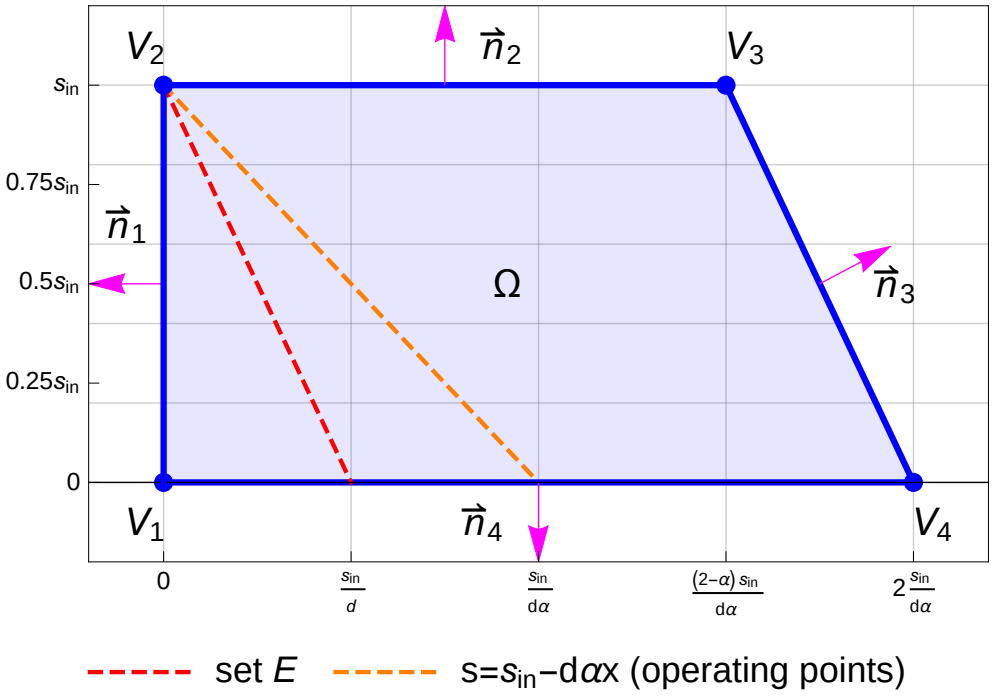

Figure 2.1: Set Ω, and the normal vectors in its boundaries.

(a) $x = 0$, $s \in [0, s_{in}]$. Its associated $\vec{v}$ and $\vec{n}$ are

$$\vec{v}_1 = \begin{bmatrix} 0 \\ u(s_{in} - s) \end{bmatrix} \text{ and } \vec{n}_1 = \begin{bmatrix} -1 \\ 0 \end{bmatrix}.$$

And their scalar product results in

$$\vec{v}_1 \cdot \vec{n}_1 = 0. \tag{2.30}$$

(b) $s = s_{in}$, $x \in \left[0, \frac{(2-\alpha)s_{in}}{d\alpha}\right]$. Its asociated $\vec{v}$ and $\vec{n}$ are

$$\vec{v}_2 = \begin{bmatrix} -(\alpha u - \mu(s_{in}))x \\ -d\mu(s_{in})x \end{bmatrix} \text{ and } \vec{n}_2 = \begin{bmatrix} 0 \\ 1 \end{bmatrix}.$$

And their scalar product results in

$$\vec{v}_2 \cdot \vec{n}_2 = -d\mu(s_{in})x \leq 0. \tag{2.31}$$

(c) Isolating s in (2.25) ($\beta(s) = x$) it can be obtained the boundary $s = 2\frac{s_{in}}{\alpha} - dx$, $x \in \left[\frac{(2-\alpha)s_{in}}{d\alpha}, \frac{2s_{in}}{d\alpha}\right]$. The normal vector can be obtained by calculating the gradient to $h(x,s) = s - 2\frac{s_{in}}{\alpha} + dx$, i.e., $\nabla h(x,s) = d\hat{\imath} + \hat{\jmath}$. Then, its asociated $\vec{v}$ and $\vec{n}$ are

$$\vec{v}_3 = \begin{bmatrix} -\left(\alpha u - \mu\left(s\right)\right)x \\ -d\mu\left(s\right)x + u\left(s_{in}\left(1 - \frac{2}{\alpha}\right) + dx\right) \end{bmatrix} \text{ and } \vec{n}_3 = \begin{bmatrix} d \\ 1 \end{bmatrix}.$$

And their scalar product results in

$$\begin{aligned} \vec{v}_3 \cdot \vec{n}_3 &= -d\alpha u x + d\mu\left(s\right)x - d\mu\left(s\right)x + u\left(s_{in}\left(1 - \frac{2}{\alpha}\right) + dx\right), \\ &= u\left(s_{in}\left(1 - \frac{2}{\alpha}\right) + dx - d\alpha x\right), \\ &= -u\left(s_{in}\left(\frac{2}{\alpha} - 1\right) - \left(1 - \alpha\right)dx\right), \end{aligned}$$

if x is replaced by its equivalent in the boundary $x = \frac{2s_{in} - \alpha s}{d\alpha}$, it is obtained

$$\begin{aligned} \vec{v}_3 \cdot \vec{n}_3 &= -u\left(s_{in}\left(\frac{2}{\alpha} - 1\right) - \left(1 - \alpha\right)\frac{2s_{in} - \alpha s}{\alpha}\right), \\ &= -u\left(s_{in}\left(\frac{2}{\alpha} - 1 - \frac{2}{\alpha} + 2\right) + \left(1 - \alpha\right)s\right), \end{aligned}$$

which finally implies the negativity of the dot product.

$$\vec{v}_3 \cdot \vec{n}_3 = -u\left(s_{in} + \left(1 - \alpha\right)\right) \leq 0. \tag{2.32}$$

(d) $s = 0$, $x \in \left[0, \frac{2s_{in}}{d\alpha}\right]$. Its asociated $\vec{v}$ and $\vec{n}$ are

$$\vec{v}_4 = \begin{bmatrix} -\alpha u x \\ u s_{in} \end{bmatrix} \text{ and } \vec{n}_4 = \begin{bmatrix} 0 \\ -1 \end{bmatrix}.$$

And their scalar product results in

$$\vec{v}_4 \cdot \vec{n}_4 = -u s_{in} \leq 0. \tag{2.33}$$

2. **Vertexes:**

(a) In $V_1(0,0)$ the vectorial field is

$$\vec{v}(V_1) = \begin{bmatrix} 0 \\ u s_{in} \end{bmatrix}, \tag{2.34}$$

which is tangent to boundary 1 and points in the correct direction. It implies that trajectories cannot leave Ω by crossing V_1.

(b) In $V_2(0, s_{in})$ the vectorial field is

$$\vec{v}(V_2) = \begin{bmatrix} 0 \\ 0 \end{bmatrix}. \tag{2.35}$$

Because it is an equilibrium point, trajectories cannot leave Ω by crossing V_2.

(c) In $V_3 \left(\frac{(2-\alpha)s_{in}}{d\alpha}, s_{in} \right)$ the vectorial field is

$$\vec{v}(V_3) = \begin{bmatrix} -(\alpha u - \mu(s_{in}))\frac{(2-\alpha)s_{in}}{d\alpha} \\ -\mu(s_{in})\frac{(2-\alpha)s_{in}}{d\alpha} \end{bmatrix}, \tag{2.36}$$

There are two cases: $u = 0$ and $u > 0$.

- For $u = 0$, it is obtained

$$\vec{v}(V_3)|_{u=0} = \begin{bmatrix} \mu(s_{in})\frac{(2-\alpha)s_{in}}{d\alpha} \\ -\mu(s_{in})\frac{(2-\alpha)s_{in}}{d\alpha} \end{bmatrix}, \tag{2.37}$$

  which is tangent to boundary 3 ($\vec{v}(V_3)|_{u=0} \cdot \vec{v_3} = 0$) and points in the correct direction (the components are positive in the $x - axis$ and negative in the $s - axis$).

- For $u > 0$, it is obtained

$$\vec{v}(V_3)|_{u>0} = \begin{bmatrix} -(\alpha u - \mu(s_{in}))\frac{(2-\alpha)s_{in}}{d\alpha} \\ -\mu(s_{in})\frac{(2-\alpha)s_{in}}{d\alpha} \end{bmatrix}. \tag{2.38}$$

  When $u > 0$, it maps the $x - axis$ component of the vector to $u \in (0, \infty) \mapsto \left(\mu(s_{in})\frac{(2-\alpha)s_{in}}{d\alpha}, -\infty \right)$. Then, as the $s - axis$ component of the vector is constant and negative, $\vec{v}(V_3)|_{u>0}$ points inside Ω.

Previous analysis implies that trajectories cannot leave Ω by crossing V_3.

(d) In $V_4 \left(\frac{2s_{in}}{d\alpha}, 0 \right)$ the vectorial field is

$$\vec{v}(V_4) = \begin{bmatrix} -2u\frac{s_{in}}{d} \\ us_{in} \end{bmatrix}. \tag{2.39}$$

There are two cases: $u = 0$ and $u > 0$.

- For $u = 0$, it is obtained

$$\vec{v}(V_4)|_{u=0} = \begin{bmatrix} 0 \\ 0 \end{bmatrix}, \tag{2.40}$$

  it corresponds to an equilibrium point, then trajectory holds in the vertex.

- For $u > 0$, it is obtained

$$\vec{v}(V_4)|_{u>0} = \begin{bmatrix} -2u\frac{s_{in}}{d} \\ us_{in} \end{bmatrix}. \tag{2.41}$$

  Whichever u is, the direction of the vector is the same. It defines a line with slope $-\frac{d}{2}$ (dividing $s - axis$ component by $x - axis$ component), which in Ω is under boundary 3. Then, the vector points inside Ω.

From the previous analysis it is inferred that trajectories cannot leave Ω by crossing V_4.

Equations (2.30), (2.31), (2.32) and (2.33) show that $\vec{v} \cdot \vec{n} \leq 0$ in all set boundaries, which implies that condition (2.26) is satisfied. And also it was proof that trajectories cannot leave the set by its vertexes. Therefore Ω is a positive invariant set. ■

Chapter 3

Continuous Stirred Tank Reactor: Controller Design

In this section, it is taken the model (1.1) in the limit case $\alpha = 1$ is considered, which is known as Continuous Stirred Tank Reactor and has been widely studied, e.g., Andrews (1968), Antonelli and Astolfi (2000), Lara-Cisneros et al. (2012) and Schaum et al. (2012) present its main properties. However, for our purposes, it is convenient to recall some of them by making the basic calculations. With $\alpha = 1$ the model adopts the following structure and its diagram is presented in Figure 3.1.

$$\begin{aligned} \dot{x} &= (-u + \mu(s))x, \\ \dot{s} &= -d\mu(s)x + u(s_{in} - s), \\ Q &= q\mu(s)x. \end{aligned} \tag{3.1}$$

A control law for reaching the optimal operating point of (3.1) is proposed, i.e., it is designed

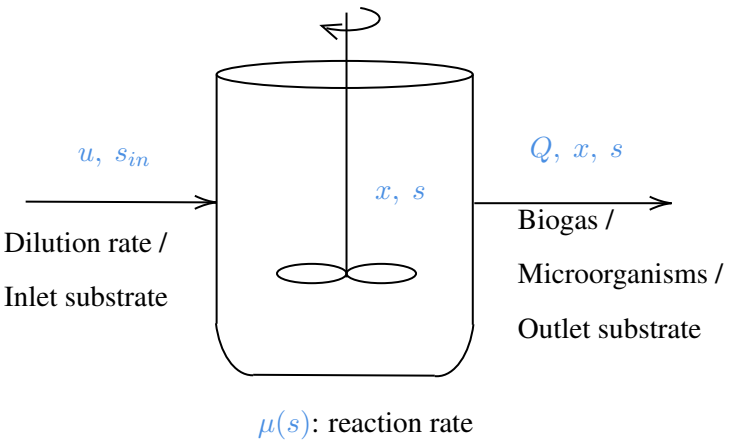

Figure 3.1: Continuos Stirred Tank Reactor diagram.

an algorithm to maximize Q by assuming that it is the only measurable variable. The idea behind the controller is quite simple, and it can be expressed as follows.

Assume that there are only two control values, labeled u_L and u_H, and at the beginning t_0 one of them (u_L or u_H) is applied, with which the system evolves during a small time $T_1 = t_1 - t_0$. It is clear that there are two measurements of the output: $Q(t_0)$ and $Q(t_1)$, with which the tendency of biogas production can be checked by computing $\text{sign}(Q(t_1) - Q(t_0))$. There are three cases,

- $\text{sign}(Q(t_1) - Q(t_0)) = -1$: Biogas production is decreasing which implies the applied input is wrong, then it is necessary to change its value.
- $\text{sign}(Q(t_1) - Q(t_0)) = 0$: Biogas production is constant which implies the system could have achieved a transient maximum or the optimal biogas production, however it is not for sure that it is the optima. In this case, once again the control value it changed in case it was not the correct maximum.
- $\text{sign}(Q(t_1) - Q(t_0)) = 1$: this condition implies biogas production is increasing towards the desired optimal operation. In this case, the used input value continues being applied.

After this first step was carried out, the process is repeated by considering different intervals $T_2, T_3, \ldots$, after which the input is changed when $\text{sign}(Q(t_i) - Q(t_{i-1})) \leq 0$. This is how the controller works, however it is necessary to prove that it can make the trajectories achieve the optimal operating point.

The first step is putting the controller in the framework of switched control (Liberzon (2012), Bacciotti (2013)), implying the need of some switching curves $S(\bar{u})$, which are obtained from the transient-critical-points of $Q(t)$. With those curves, the controller is formalized, and it is demonstrated that it guarantees global convergence to a neighborhood of the optimal operating point. It should be independent of the reaction rate and the parameter uncertainty.

3.1 Curves in which biogas achieves transient extrema: $S(\bar{u})$

For control purposes, the function $\eta(x, s, u)$ is defined as the time derivative of Q along the trajectories of system (3.1), i.e.

$$\begin{aligned}
\eta(x,s,u) &\triangleq \frac{\mathrm{d}Q}{\mathrm{d}t} = \frac{\partial Q}{\partial x}\dot{x} + \frac{\partial Q}{\partial s}\dot{s}, \\
&= q\mu(s)\dot{x} + q\frac{\mathrm{d}\mu(s)}{\mathrm{d}s}x\dot{s}, \\
&= q\mu(s)(-u + \mu(s))x + q\frac{\mathrm{d}\mu(s)}{\mathrm{d}s}x\left(-d\mu(s)x + u(s_{in} - s)\right), \\
&= qx\left(\mu(s)(-u + \mu(s)) + \frac{\mathrm{d}\mu(s)}{\mathrm{d}s}\left(-d\mu(s)x + u(s_{in} - s)\right)\right). \qquad (3.2)
\end{aligned}$$

For a constant input $\bar{u}$, the curve $S(\bar{u}) = \{(x,\, s) \in \mathbb{R}^2_{\geq 0} | \eta(x, s, \bar{u}) = 0\}$ in the phase plane consists of the transient critical points for trajectories of the system (3.1) with the input $\bar{u}$, i.e., the points where Q has a local minimum, a maximum or an inflection point for that (constant) input.

Theorem 6. *If (2.4) has only one solution in the compact $[0, s_{in}]$, all curves $S(\bar{u})$ (generated with different $\bar{u}$ values) intersect at the optimal operating point.*

Proof. Making $\eta(x, s, u) = 0$ in (3.2), and ignoring the trivial solution $x = 0$, then

$$\mu(s)(-u + \mu(s)) + \frac{\mathrm{d}\mu(s)}{\mathrm{d}s}\left(-d\mu(s)x + u(s_{in} - s)\right) = 0,$$

$$\frac{\mathrm{d}\mu(s)}{\mathrm{d}s}\left(d\mu(s)x - u(s_{in} - s)\right) = \mu(s)(-u + \mu(s)),$$

$$d\mu(s)x - u(s_{in} - s) = \frac{1}{\frac{\mathrm{d}\mu(s)}{\mathrm{d}s}}\mu(s)(-u + \mu(s)),$$

$$x = \frac{1}{d\frac{\mathrm{d}\mu(s)}{\mathrm{d}s}}(-u + \mu(s)) + \frac{u}{d\mu(s)}(s_{in} - s),$$

$$x = \frac{u}{d}\left(\frac{s_{in} - s}{\mu(s)} - \frac{1}{\frac{\mathrm{d}\mu(s)}{\mathrm{d}ds}}\right) + \frac{\mu(s)}{d\frac{\mathrm{d}\mu(s)}{\mathrm{d}s}}, \tag{3.3}$$

If two different values of u are taken: u_L (L: low) y u_H (H: high), there are two $S(\bar{u})$ curves

$$x_{u_L} = \frac{u_L}{d}\left(\frac{s_{in} - s}{\mu(s)} - \frac{1}{\frac{\mathrm{d}\mu(s)}{\mathrm{d}s}}\right) + \frac{\mu(s)}{d\frac{\mathrm{d}\mu(s)}{\mathrm{d}s}},$$

$$x_{u_H} = \frac{u_H}{d}\left(\frac{s_{in} - s}{\mu(s)} - \frac{1}{\frac{\mathrm{d}\mu(s)}{\mathrm{d}s}}\right) + \frac{\mu(s)}{d\frac{\mathrm{d}\mu(s)}{\mathrm{d}s}},$$

whose intersection can be checked by making $x_{u_L} = x_{u_H}$,

$$\frac{u_L}{d}\left(\frac{s_{in} - s}{\mu(s)} - \frac{1}{\frac{\mathrm{d}\mu(s)}{\mathrm{d}s}}\right) + \frac{\mu(s)}{d\frac{\mathrm{d}\mu(s)}{\mathrm{d}s}} = \frac{u_H}{d}\left(\frac{s_{in} - s}{\mu(s)} - \frac{1}{\frac{\mathrm{d}\mu(s)}{\mathrm{d}s}}\right) + \frac{\mu(s)}{d\frac{\mathrm{d}\mu(s)}{\mathrm{d}s}},$$

$$\frac{u_H - u_L}{d}\left(\frac{s_{in} - s}{\mu(s)} - \frac{1}{\frac{\mathrm{d}\mu(s)}{\mathrm{d}s}}\right) = 0,$$

$$\frac{s_{in} - s}{\mu(s)} = \frac{1}{\frac{\mathrm{d}\mu(s)}{\mathrm{d}s}},$$

$$\frac{\mathrm{d}\mu(s)}{\mathrm{d}s}(s_{in} - s) = \mu(s),$$

$$\frac{\mathrm{d}\mu(s)}{\mathrm{d}s}(s_{in} - s) - \mu(s) = 0. \tag{3.4}$$

Replacing (3.4) in (3.3) it is obtained the following condition, which implies that it is an operating point:

$$x = \frac{s_{in} - s}{d}. \tag{3.5}$$

If (2.4) and (3.4) are compared, it is easy to see that they are the same equation, $\bar{s}$ and s act only like dummy variables. This implies that for a given $\mu(s)$, all $S(\bar{u})$ curves (generated with different input values) intersect at the stationary maximum of Q if (2.4) has only one solution in the compact $[0, s_{in}]$. ■

In particular, if Monod and Haldane reaction rates are considered, for some set of parameters, and using different u values, their asociated $S(\bar{u})$ curves are shown in Figure 3.2. And, as it was demonstrated, all of them intersect at the optimal operating point (x^*, s^*).

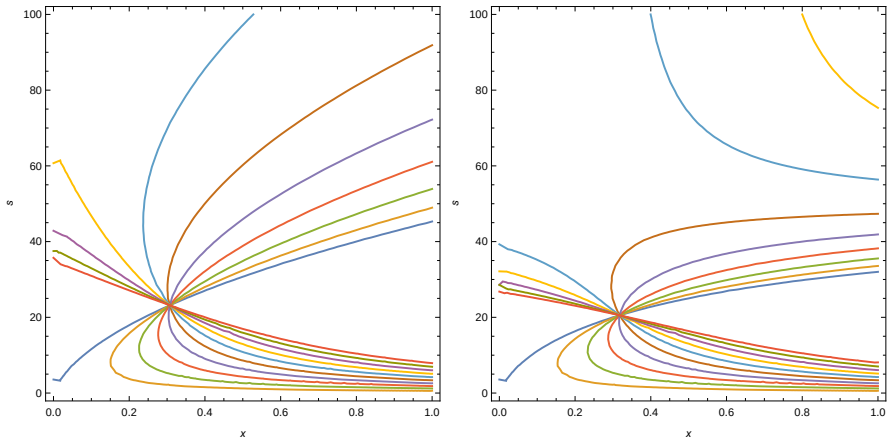

(a) Monod reaction rate. **(b)** Haldane reaction rate.

Figure 3.2: $S(\bar{u})$ curves for postive $\bar{u}$ values.

3.2 Switching curves design

Theorem 6 states that all $S(\bar{u})$ curves intersect at the optimal operating point, suggesting that the optimization of Q can be achieved by a properly switching between two of them (associated with u_L and u_H). As a first approach, a reasonable restriction could be $u_L \leq u^* \leq u_H$ because the switching between u_L and u_H has to generate u^* (on average). Nevertheless, there is another restriction imposed by saturation limits presented in Schaum et al. (2012) $u_L < \mu(s_{in})$

and $u_H > \mu_{max}$, which have to be satisfied for every saturated controller.

Figures 3.3a and 3.3b shown the open-loop phase portraits for a given $\bar{u}$ for both reaction rates, and also their associated switching curves $S(\bar{u})$ are presented. On one hand, for Monod kinetics (Figure 3.3a) with $\bar{u} \in (0, \mu_0)$ there is on equilibrium point (in addition to the washout), but two intersections between $S(\bar{u})$ and E. On the other hand, for Haldane reaction rate (Figure 3.3b) with $\bar{u} \in (\mu(s_{in}), \mu(s_c))$ there are two equilibrium points (in addition to the washout), but two intersections between $S(\bar{u})$ and E.

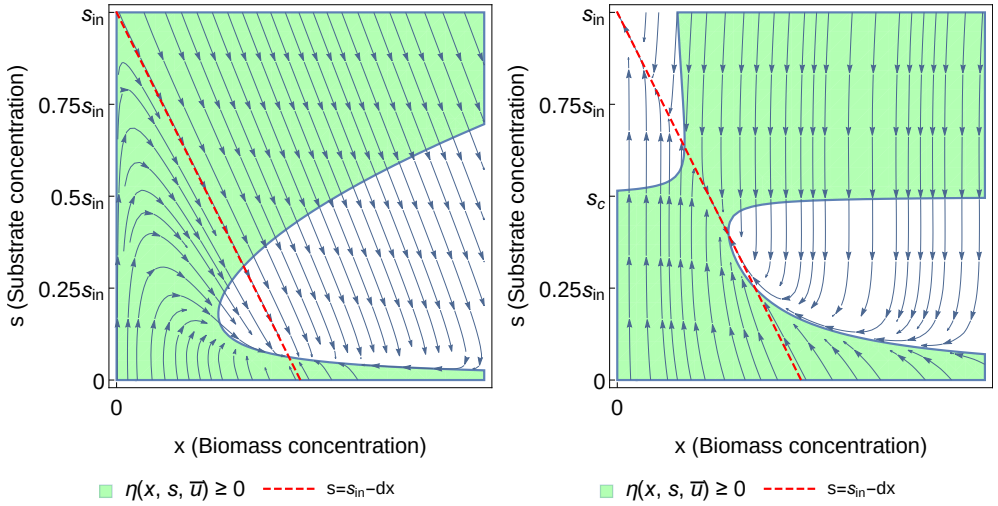

(a) Monod kinetics with $\bar{u} \in (0, \mu_0)$.

(b) Haldane kinetics with $\bar{u} \in (\mu(s_{in}), \mu(s_c))$.

Figure 3.3: Open-Loop Phase portrait with $\eta(x, s, \bar{u}) \geq 0$ and the equillibria set E.

It is easily seen that $S(\bar{u})$ curves cross, not only the optimal operating point but also the equilibria associated to $\bar{u}$. That is why it is necessary to select $S(\bar{u})$ curves that have only one intersection with the equilibria set E (2.13) to guarantee that trajectories do not get stuck in another equilibrium. Then, it is concluded that the proper way to select the admissible input values is choosing $\bar{u}$ not satisfying conditions (2.2), in order to avoid other intersections between $S(\bar{u})$ and E.

Therefore, the input values which satisfy the above conditions are

$$u_L = 0. \tag{3.6}$$

and

$$u_H > \mu_{\max}, \tag{3.7}$$

where $\mu_{\max} = \mu(s_{in})$ for Monod and $\mu_{\max} = \mu(s_c)$ for Haldane kinetics. Figures 3.4a and 3.4b, present system trajectories considering $\bar{u} = u_L$. As it can be seen, the curve $S(u_L)$ has

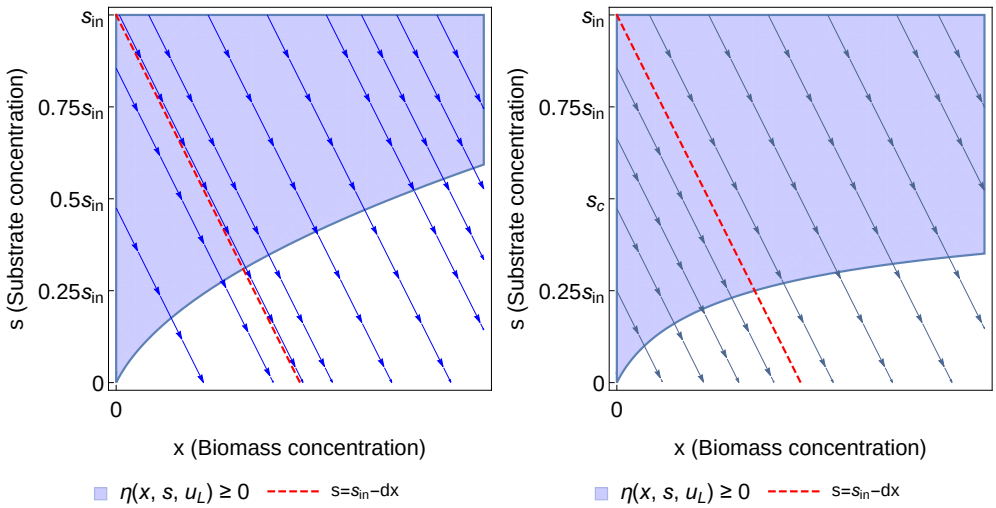

(a) Monod reaction rate.

(b) Haldane reaction rate.

Figure 3.4: Phase portrait with $\eta(x, s, u_L) \geq 0$ and the equilibria set E ($u_L = 0$).

only one intersection with the set E as desired. Figures 3.5a and 3.5b shown phase planes for $\bar{u} = u_H$. Once again, the curve $S(u_H)$ has only one intersection with the set E, which guarantee proper switching curves.

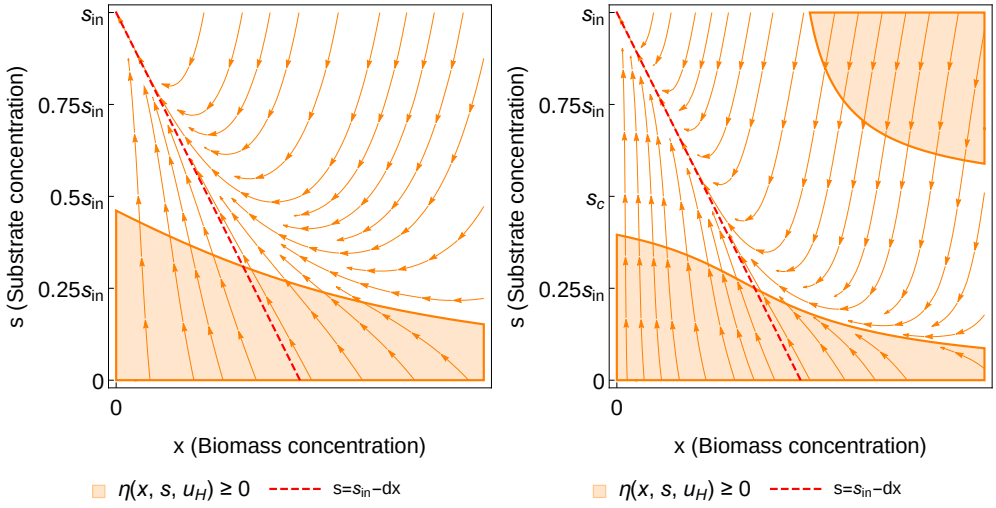

(a) Monod reaction rate.

(b) Haldane reaction rate.

Figure 3.5: Phase portrait with $\eta(x, s, u_H) \geq 0$ and the equilibria set E ($u_H > \mu_{\max}$).

3.2.1 Closed-Loop Dynamics

Figure 3.6 displays the closed-loop phase plane for the bioreactor, i.e., the system behavior by mixing both input values u_L and u_H is presented, in order to understand how trajectories behave. We can sat that this is the heart of the proposed optimization strategy.

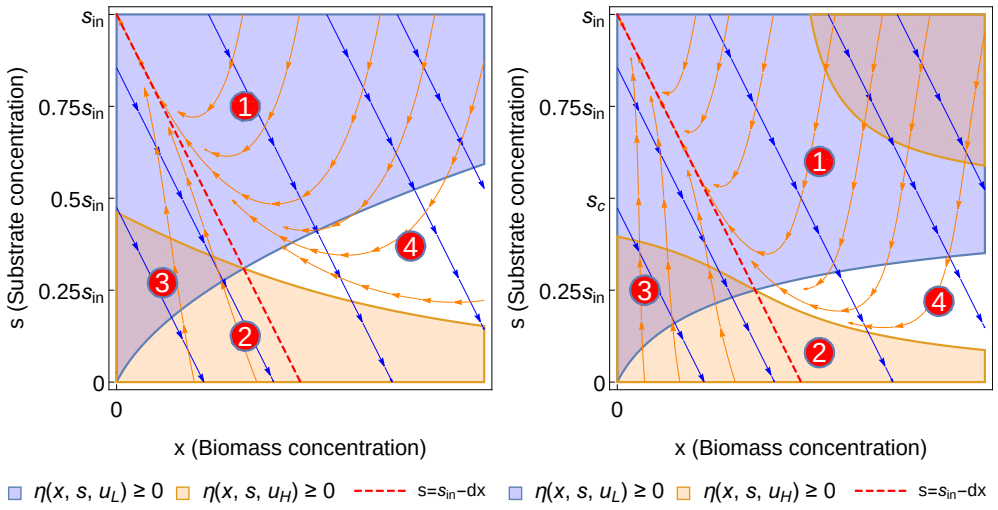

(a) Monod reaction rate.

(b) Haldane reaction rate.

Figure 3.6: Phase portrait for complete dynamics with $u_L = 0$ and $u_H > \mu_{\max}$ $(\alpha = 1)$.

3.3 Sample-and-Hold Solutions

Instead of using Filippov solution's notion for differential equations, it is used the concept of Sample-and-Hold solutions presented by Cortes (2008). For a more detailed explanation consult Clarke et al. (1997). This is useful for differential equations with discontinuous inputs because the differential equation with discontinuous right-hand-side can be analysed without the need to consider the resulting differential inclusion.

Let $f : \mathbb{R}^n \times \mathbb{U} \to \mathbb{R}^n$, where $\mathbb{U} \subseteq \mathbb{R}^m$ is the set of allowable control-function values, and consider the control equation on $\mathbb{R}^n$ given by

$$\dot{x}(t) = f(x(t), u). \tag{3.8}$$

The first step is selecting the control input in some set, either an open loop $u : [0, \infty) \to \mathbb{U}$, a closed-loop $u : \mathbb{R}^n \to \mathbb{U}$, or a combination $u : [0, \infty) \times \mathbb{R}^n \to \mathbb{U}$, and then consider the resulting differential equation.

A *partition* of the interval $[t_0, t_N]$ is an increasing sequence $\pi = \{t_i\}_{i=0}^{N}$, i.e., $t_0 < t_1 < t_2 < \cdots < t_N$. The partition need not to be finite. The notion of partition of $[t_0, \infty)$ is defined similarly. The diameter of π is $\mathrm{diam}(\pi) \triangleq \sup\{t_i - t_{i-1} : i \in \{1, \ldots, N\}\}$. Given a control input $u :\in [0, \infty) \times \mathbb{R}^n \to \mathbb{U}$, an initial condition x_0, and a partition π of $[t_0, t_1]$, a $\pi - solution$ of (3.8) defined on $[t_0, t_1] \subset \mathbb{R}$ is the map $x : [t_0, t_1] \to \mathbb{R}^n$, with $x(t_0) = x_0$, recursively defined by requiring the curve $t \in [t_{i-1}, t_i] \mapsto x(t)$, for $i \in \{1, \ldots, N-1\}$, to be a Carathéodory solution of the differential equation

$$\dot{x}(t) = f(x(t), u(t_{i-1}, x(t_{i-1}))). \tag{3.9}$$

$\pi - solutions$ are also referred to as sample-and-hold solutions because the control is held fixed throughout each interval of the partition at the value according to the state at the beginning of the interval Cortes (2008).

Clarke et al. (1997) remarked that this notion of solution is quite different from the *Euler solution* which would be obtained when attempting to solve differential equation (3.8) using Euler's method: in that case, on each interval $t \in [t_{i-1}, t_i]$ one would have the formula $x(t) = x(t_{i-1}) + (t - t_{i-1}) f(x(t_{i-1}), u(t_{i-1}, x(t_{i-1})))$, corresponding to the solution of the differential equation $\dot{x}(t) = f(x(t_{i-1}), u(t_{i-1}, x(t_{i-1})))$. This alternative definition does not have any physical meaning in terms of the original system.

3.4 Fast Extremum Seeking Controller

Conditions for proper switching curves were obtained; the proposed control law is defined as a switching system (see e.g. Bacciotti (2013), Liberzon (2012)) alternating between systems Σ_1 and Σ_2, and having as switching surfaces $S_1 = \{(x, s) | \eta(x, s, u_L) = 0\}$ and $S_2 = \{(x, s) | \eta(x, s, u_H) = 0\}$. However, its behavior is very different with respect to the others, because the switching event occurs whenever the slop of $Q(t)$ is negative or zero (when the biogas is decreasing or achieving an stationary maximum), and not only when the state crosses a switching surface.

Definition 7. ***(Controller)*** *Define* $\Omega_1 = \{\eta(x, s, u_L) > 0\}$, $\Omega_2 = \{\eta(x, s, u_H) > 0$, *(for non-monotonic* $\mu(s)$, $s < s_c)\}$ *and introduce the discrete state* σ, *whose role is to specify, at each time instant* $t \geq 0$, *the index* $\sigma \in \{1, 2\}$ *of the active system. Let* $\sigma(t_0) = 1$ *and define* $\pi = \{t_i\}_{i=0}^{\infty}$ *as a partition of* $[0, \infty)$, *with a very small diameter* $\mathrm{diam}(\pi) \triangleq \sup_{i \in \{1,2,\ldots\}}(t_i - t_{i-1})$.

At the beginning, let the system evolve as Σ_1 *in the interval* $[t_0, t_1]$. *Then, for each* $t_i \geq t_1$, *if* $\sigma(t_{i-1}) = j \in \{1, 2\}$ *and* $(x(t_i), s(t_i)) \in \Omega_j$, *make* $\sigma(t_i) = j$. *On the other hand, if* $\sigma(t_{i-1}) = 1$ *but* $(x(t_i), s(t_i)) \notin \Omega_1$, *let* $\sigma(t_i) = 2$. *In the same way, if* $\sigma(t_{i-1}) = 2$ *but* $(x(t), s(t)) \notin \Omega_2$, *let* $\sigma(t_i) = 1$. *It is said that a switching event occurs when* σ *changes its value.*

The closed loop trajectories, generated with this algorithm, can be understood as the $\pi -$ solutions of 3.1 by defining recursively the applied input (u_L or u_H). △

The previous definition expresses the following system behavior: at the beginning it is applied u_L as an initial condition. The signum of $\frac{\mathrm{d}Q}{\mathrm{d}t}$ is checked at every instant t_i and when $\frac{\mathrm{d}Q}{\mathrm{d}t}|_{t=t_i} \leq 0$, the input value u is switched. It means that it is desired to search the optimal operating point by making Q grow as much as possible, or by making Q decrease in a proper way. The properties of Controller in Definition 7 in the nominal case are given in Theorem 8.

Theorem 8. *Assume that $\mu(s)$ is at least once differentiable and it satisfies one of the following statements:*

- *$\mu(s)$ is concave monotonic increasing.*
- *$\mu(s)$ is convex monotonic increasing.*
- *$\mu(s)$ has only one maximum in $s_c \in (0, s_{in})$, it is concave monotonic increasing in $[0, s_c]$, and monotonic decreasing in $[s_c, s_{in}]$.*

Consider the Controller in Definition 7, system (3.1) and consider that the $\mathrm{sign}(\frac{\mathrm{d}Q}{\mathrm{d}t})$ is available for measurement. Given a neighborhood of the optimal operating point, there exists π^* such that if $\mathrm{diam}(\pi) < \mathrm{diam}(\pi^*)$ the system trajectories achieve it asymptotically for any initial condition $(x(0),\ s(0)) \in \Omega$ $(x(0) \neq 0)$.

Proof. Define the following regions: $R_1 = \Omega_1 \cap \Omega_2^c$, $R_2 = \Omega_1^c \cap \Omega_2$, $R_3 = \Omega_1 \cap \Omega_2$ and $R_4 = \Omega_1^c \cap \Omega_2^c$. The proof is based on the following statements.

- Theorem 6: all $S(\bar{u})$ curves intersect at the optimal operating point.
- Lemma 9: Assume that $\mu(s)$ is at least once differentiable and it satisfies one of the following statements:
  - $\mu(s)$ is concave monotonic increasing.
  - $\mu(s)$ is convex monotonic increasing.
  - $\mu(s)$ has only one maximum in $s_c \in (0, s_{in})$, it is concave monotonic increasing in $[0, s_c]$, and monotonic decreasing in $[s_c, s_{in}]$.

S_1 and S_2 divide the state space in four regions R_1, R_2, R_3 and R_4, which are oriented clockwise $R_1 - R_4 - R_2 - R_3$ as shown in Figure 3.6.

- Lemma 10: system trajectories starting in R_1 or R_2 reach R_3 or R_4 in finite time.
- Lemma 11: system trajectories starting in R_3 or R_4 remain in a neighborhood of R_3 or R_4, respectively.
- Lemma 12: system trajectories starting in R_3 or R_4 converge to a neighborhood of the optimal operating point asymptotically.

■

Lemma 9. *Assume that $\mu(s)$ is at least once differentiable and it satisfies one of the following statements:*

- *$\mu(s)$ is concave monotonic increasing.*
- *$\mu(s)$ is convex monotonic increasing.*
- *$\mu(s)$ has only one maximum in $s_c \in (0, s_{in})$, it is concave monotonic increasing in $[0, s_c]$, and monotonic decreasing in $[s_c, s_{in}]$.*

S_1 and S_2 divide the state space in four regions R_1, R_2, R_3 and R_4, which are oriented clockwise as $R_1 - R_4 - R_2 - R_3$ as shown in Figure 3.6.

Proof. Conditions to ensure that $\eta(x, s, u) > 0$ are obtained at the beginning; $\eta(x, s, u) > 0$ has the following representation:

$$\eta(x, s, u) = qx \left(\mu(s)(-u + \mu(s)) + \frac{\mathrm{d}\mu(s)}{\mathrm{d}s} \left(-d\mu(s)x + u(s_{in} - s)\right) \right) > 0.$$

There are two cases for the inequality (when $x > 0$ is considered):

1. If $\mu'(s) > 0$:
$$x < \frac{u_H}{d} \left(\frac{s_{in} - s}{\mu(s)} - \frac{1}{\mu'(s)} \right) + \frac{\mu(s)}{d\mu'(s)}. \tag{3.10}$$
2. If $\mu'(s) < 0$:
$$x > \frac{u_H}{d} \left(\frac{s_{in} - s}{\mu(s)} - \frac{1}{\mu'(s)} \right) + \frac{\mu(s)}{d\mu'(s)}. \tag{3.11}$$

Below each $\mu(s)$ behavior is considered, and both curves, $S_1 = S(u_L)$ and $S_2 = S(u_H)$, are analysed in each case.

- $\mu(s)$ is monotonic increasing concave.

  The behavior of this function and its derivative, which is monotonic decreasing because its concavity is negative, are shown in Figure 3.7. For both switching curves, the region in which $\eta(x, s, u) > 0$ is under the curve.

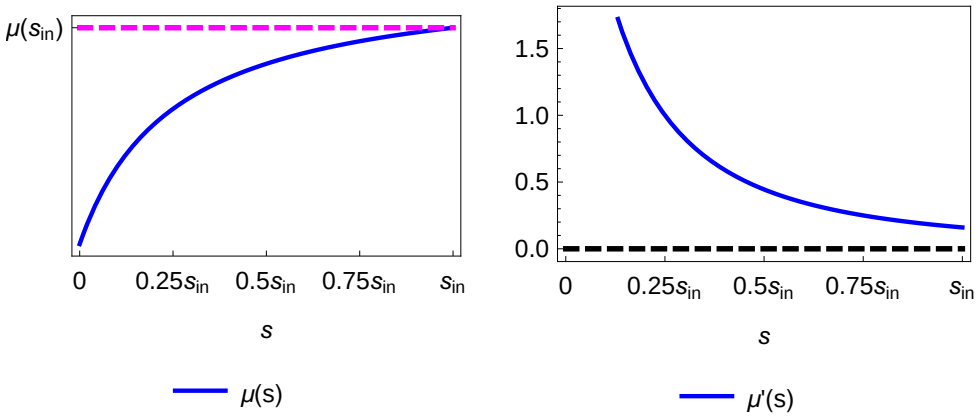

Figure 3.7: Concave monotonic increasing $\mu(s)$.

  – **Analysis of** S_1. The curve S_1 has the following representation:

$$x = \frac{\mu(s)}{d\mu'(s)}.$$

  As $\mu(s)$ grows while $\mu'(s)$ decreases, the quotient $\frac{\mu(s)}{d\mu'(s)}$ grows faster as s increases. Since $\mu(0) = 0$ and for the previous properties, $x(s)$ is convex and it crosses the origin as in Figure 3.8.

  – **Analysis of** S_2. The curve S_2 has the following representation:

$$x = \frac{u_H}{d}\left(\frac{s_{in} - s}{\mu(s)} - \frac{1}{\mu'(s)}\right) + \frac{\mu(s)}{d\mu'(s)}.$$

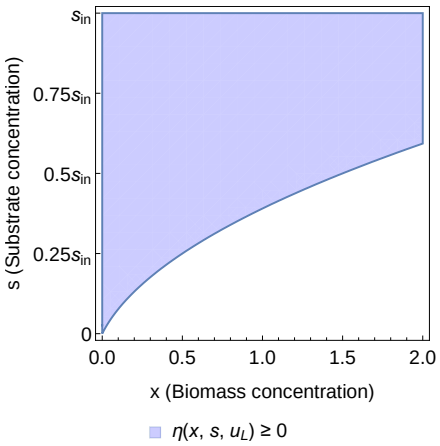

Figure 3.8: S_1 for concave monotonic increasing $\mu(s)$.

The $\lim_{s \to 0^+} x = \infty$, and since $u_H > \mu(s_{in})$, $x(s_{in}) = -\frac{u_H - \mu(s_{in})}{d\mu'(s_{in})} < 0$. Therefore there is an intersection with the s axis in $(0, s_{in})$. The switching curve form is shown in Figure 3.9.

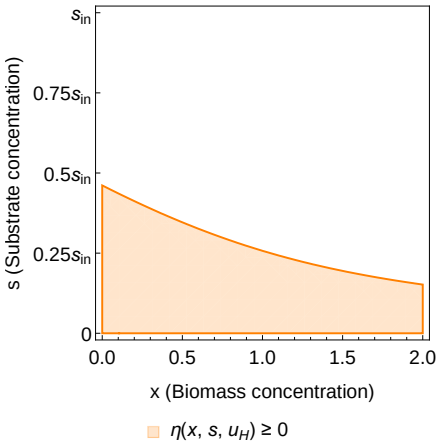

Figure 3.9: S_2 for concave monotonic increasing $\mu(s)$.

Both curves with their associated regions in which $\eta(x, s, u) > 0$ are presented in Figure 3.10.

- $\mu(s)$ is convex monotonic increasing.

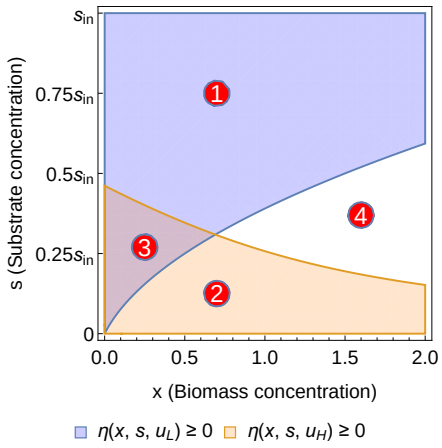

Figure 3.10: Regions for concave monotonic increasing $\mu(s)$.

The behavior of this function and its derivative, which is monotonic increasing because its concavity is positive, are shown in Figure 3.11. For both switching curves, the region in which $\eta(x, s, u) > 0$ is under the curve.

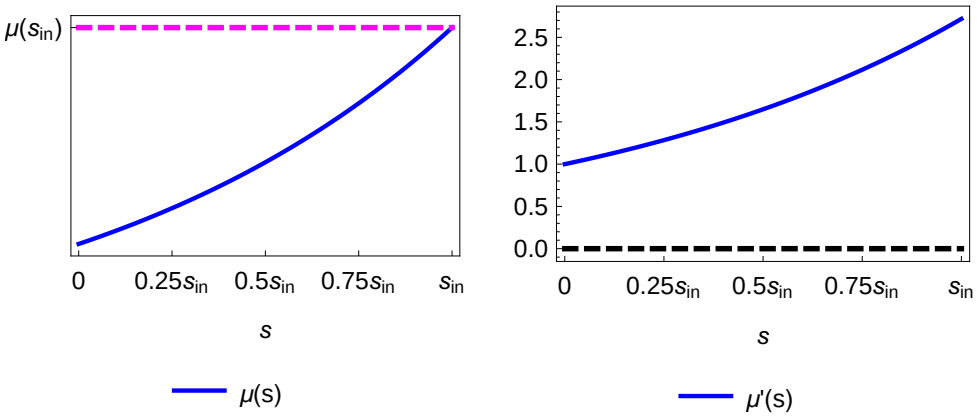

Figure 3.11: Convex monotonic increasing $\mu(s)$.

– **Analysis of** S_1. The curve S_1 has the following representation:

$$x = \frac{\mu(s)}{d\mu'(s)}.$$

As $\mu(s)$ grows while $\mu'(s)$ increases, the quotient $\frac{\mu(s)}{d\mu'(s)}$ grows slower as s increases. Since $\mu(0) = 0$ and for the previous properties, $x(s)$ is concave and it crosses the origin as in Figure 3.12.

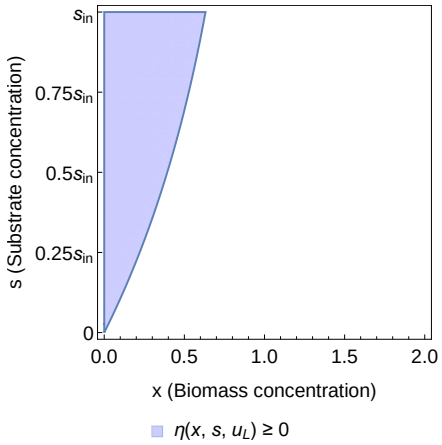

Figure 3.12: S_1 for convex monotonic increasing $\mu(s)$.

– **Analysis of** S_2. The curve S_2 has the following representation:

$$x = \frac{u_H}{d}\left(\frac{s_{in} - s}{\mu(s)} - \frac{1}{\mu'(s)}\right) + \frac{\mu(s)}{d\mu'(s)}.$$

The $\lim_{s\to 0^+} x = \infty$, and since $u_H > \mu(s_{in})$, $x(s_{in}) = -\frac{u_H - \mu(s_{in})}{d\mu'(s_{in})} < 0$. Therefore there is an intersection with the s axis in $(0, s_{in})$. The switching curve form is shown in Figure 3.13.

Both curves with their associated regions in which $\eta(x, s, u) > 0$ are presented in Figure **??**.

- $\mu(s)$ has only one maximum in $s_c \in (0, s_{in})$, it is concave monotonic increasing in $[0, s_c]$, and monotonic decreasing in $[s_c, s_{in}]$.

The behavior of this function and its derivative, which is monotonic decreasing in $[0, s_c)$ and negative in $(s_c, s_{in}]$, are shown in Figure 3.15.

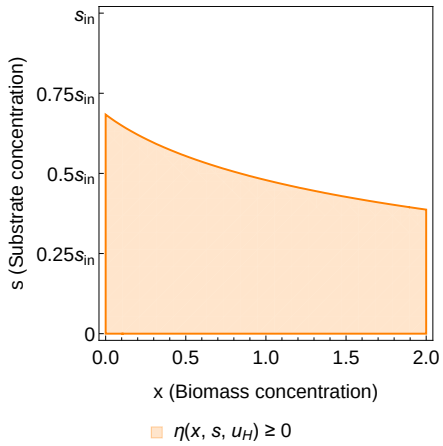

Figure 3.13: S_2 for convex monotonic increasing $\mu(s)$.

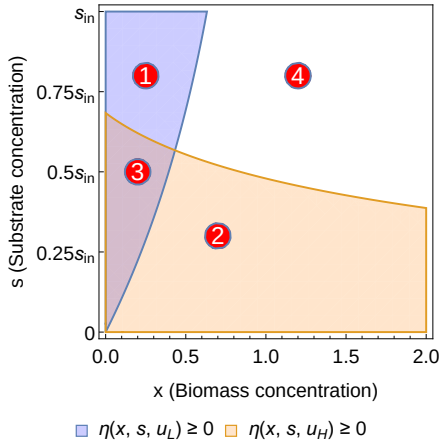

Figure 3.14: Regions for convex monotonic increasing $\mu(s)$.

– **Analysis of** S_1. The curve S_1 has the following representation:

$$x = \frac{\mu(s)}{d\mu'(s)}.$$

For $s \in [0, s_c)$, $\mu(s)$ grows while $\mu'(s)$ decreases, the quotient $\frac{\mu(s)}{d\mu'(s)}$ grows faster as s increases. However, in $(s_c, s_{in}]$, $\mu'(s)$ is negative and there are not curve in $x > 0$. Since $\mu(0) = 0$, $\lim_{s \to s_c} x$, and for the previous properties, $x(s)$ it crosses the origin and its form is shown in Figure 3.16. The region in which $\eta(x, s, u_L) > 0$ is under the curve for $s \in [0, s_c)$, and over the x axis for $s \in [s_c, s_{in}]$ ($\eta(x, s_c, u_L) =$

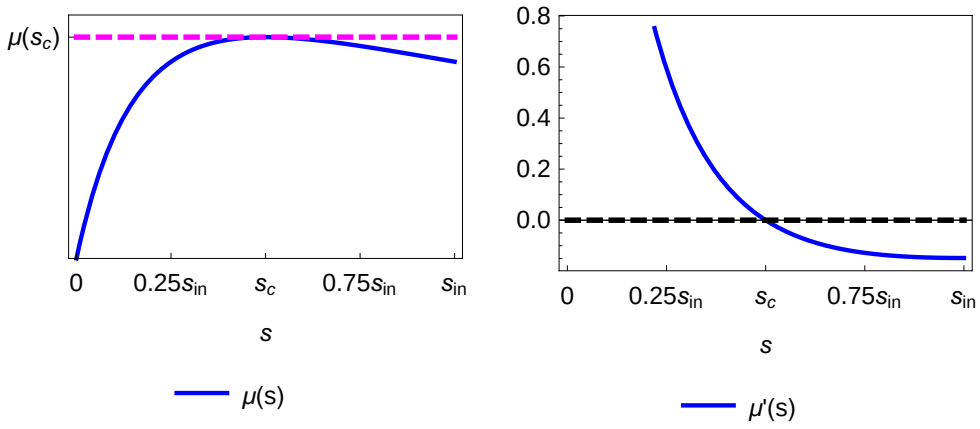

Figure 3.15: Haldane-like $\mu(s)$.

$qx\mu^2(s_c) > 0$, and $\mu'(s) < 0\ \forall s \in (s_c, s_{in})$).

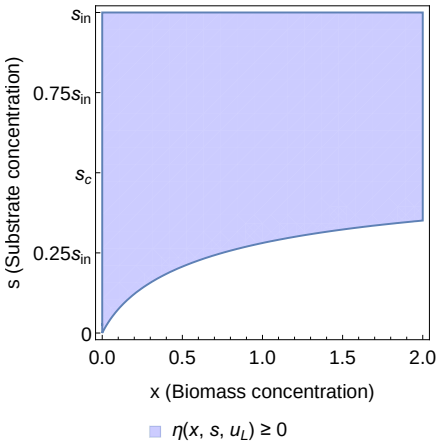

Figure 3.16: S_1 for Haldane-like $\mu(s)$.

– **Analysis of** S_2. The curve S_2 has the following representation:

$$x = \frac{u_H}{d}\left(\frac{s_{in} - s}{\mu(s)} - \frac{1}{\mu'(s)}\right) + \frac{\mu(s)}{d\mu'(s)}.$$

The $\lim_{s\to 0^+} x = \lim_{s\to s_c^+} x = \infty$, $\lim_{s\to s_c^-} x = -\infty$, and since $u_H > \mu(s_{in})$, $x(s_{in}) = -\frac{u_H - \mu(s_{in})}{d\mu'(s_{in})} > 0$. Therefore, there is an intersection with the s axis in $(0, s_c)$ and

an asymptote in s_c. The region in which $\eta(x, s, u) > 0$ is under the curve in $[0, s_c)$ and over the curve in $(s_c, s_{in}]$. This switching curve form is shown in Figure 3.17.

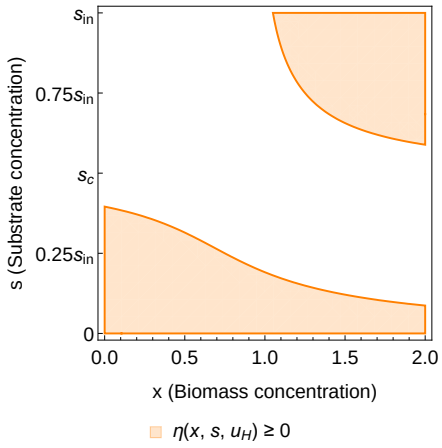

Figure 3.17: S_2 for Haldane-like $\mu(s)$.

Both curves with their associated regions in which $\eta(x, s, u) > 0$ are presented in Figure 3.18.

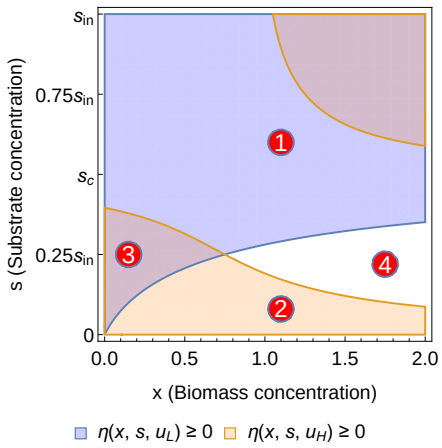

Figure 3.18: S_2 for Haldane-like $\mu(s)$.

Previous analysis is also valid for a monotonic increasing line $\mu(s) = ks$ ($k \in \mathbb{R}$). Therefore the state space is divided in four regions oriented clockwise $R_1 - R_4 - R_2 - R_3$. ■

Lemma 10. *System trajectories starting in R_1 or R_2 reach R_3 or R_4 in finite time.*

Proof. The following coordinate change is introduced, in order to make the analysis easier

$$z_1 = x, \tag{3.12}$$

$$z_2 = dx + s. \tag{3.13}$$

Bioreactor dynamics (3.1) in new coordinates has the following representation.

$$\dot{z}_1 = -\left(u - \mu(z_2 - dz_1)\right) z_1, \tag{3.14}$$

$$\dot{z}_2 = -\left(z_2 - s_{in}\right) u. \tag{3.15}$$

and therefore, Σ_1 and Σ_2 are as follows

$$\Sigma_1 : \begin{cases} \dot{z}_1 = \mu(z_2 - dz_1)z_1, \\ \dot{z}_2 = 0. \end{cases} \tag{3.16}$$

For Σ_1, z_1 increases and z_2 is maintained constant.

$$\Sigma_2 : \begin{cases} \dot{z}_1 = -(u_H - \mu(z_2 - dz_1))z_1, \\ \dot{z}_2 = -\left(z_2 - s_{in}\right) u_H. \end{cases} \tag{3.17}$$

For Σ_2, z_1 decreases and z_2 has three different options

1. If $z_2 < s_{in}$, z_2 increases.
2. If $z_2 = s_{in}$, z_2 is constant.
3. If $z_2 > s_{in}$, z_2 decreases.

For completeness of the proof, it is necessary to recover the form of previous axes and all sets in the new coordinates.

- Mapping $x = 0$ (axis s):

  $$z_1 = 0,$$

  $$z_2 = s.$$

  Which implies that s and z_2 axes are coincident.

- Mapping $s = 0$ (axis x):

$$z_2 \quad = \quad dz_1$$

  Which implies that x axis is a line with slope d that crosses the origin.

- The set of equilibria E (2.13) is easier in new coordinates.

$$E = \{(z_1,\, z_2) \in \mathbb{R}^2_{\geq 0} | z_2 = s_{in}\}. \tag{3.18}$$

Phase planes presented in Figure 3.6 were constructed by mixing Figures 3.4 and 3.5. Same plots, but in new coordinates, are presented in Figure 3.19, in order to graphically understand the coordinates change. It can be seen that the state space is divided in four operating regions,

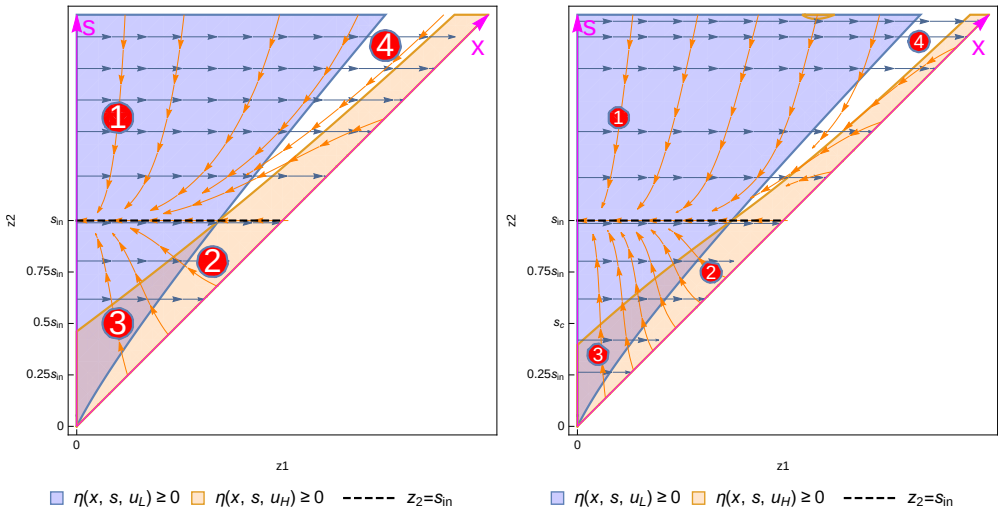

(a) Monod reaction rate.

(b) Haldane reaction rate.

Figure 3.19: Phase portrait with $u_L = 0$ and $u_H > \mu_{\max}$ in z coordinates.

independently of the reaction rate. To ensure convergence, it is necessary to analyse all of them, considering initial conditions inside each one and looking at how trajectories behave. Also, it is necessary to remember that $u(t_0) = u_L$, and that π is sufficiently small that trajectories move very little during each interval $[t_{i-1}, t_i]$ $i \in \{1, 2, \dots\}$.

Region 1 (R_1). It was stated that $\sigma(t_0) = 1$, therefore the active system is Σ_1 and $(z_1, z_2) \in \Omega_1$, which implies that z_1 grows while z_2 remains constant. Then, there are three possibilities:

1. If $z_2 \leq s_{in}$, trajectories go to region R_3 without a switching event, then the active system continues being Σ_1. If the trajectory is close to the optimal state the trajectory may quickly pass region R_3 and end at t_i in R_2 with a switching event to Σ_2.

2. If $z_2 = s_{in}$, trajectories arrive to the optimal operating point with a switching event (the switch can occur exactly at the optimal operating point or after passing it, as system could go to region R_2 due to the partition π), then the active system changes to Σ_2.

3. If $z_2 \geq s_{in}$, trajectories could go to R_4 with a switching event (the switch can occur exactly at the surface S_1 or after passing it, due to the partition π). If trajectory is close to the optimal state it could end in region R_2. Whichever the case is, the active system changes to Σ_2.

Region 2 (R_2). It was said that $\sigma(t_0) = 1$, then the active system is Σ_1, but $(z_1, z_2) \notin \Omega_1$. This fact produces an initial switching event to system Σ_2. When Σ_2 is the active system, z_1 decreases, and there are three cases:

1. If $z_2 < s_{in}$, z_2 grows and trajectories could go to region R_3 without a switching event, then the active system continues being Σ_2. If trajectory is close to the optimal state, it could pass to region R_1 with a switching event to Σ_1.

2. If $z_2 = s_{in}$, z_2 is maintained constant, and trajectories arrive to the optimal operating point with a switching event (the switch can occur exactly at the optimal operaitng point or after passing it, as system could go to region R_1 due to the partition π), then the active system changes to Σ_1.

3. If $z_2 > s_{in}$, trajectories could go to R_4 with a switching event (the switch can occur exactly at the surface S_2 or after passing it, due to the partition π). If trajectory is close to the optimal state it could end in region R_1. Whichever the case is, the active system changes to Σ_2.

Finite time convergence can be obtained from the fact that Σ_1 and Σ_2 have different asymptotically stable equilibrium points (they are not the optimal operating point). Since trajectories need to cross switching surfaces to achieve those equilibria, it is concluded that trajectories starting at $(z_1, z_2) \in R_1 \cup R_2$ reach $R_3 \cup R_4$ in finite time. ■

Lemma 11. *System trajectories starting in R_3 or R_4 remain in a neighborhood of R_3 or R_4, respectively.*

Proof. **Region 3** (R_3). As $\sigma(t_0) = 1$, the active system is Σ_1. Then z_1 grows, while z_2 is constant. $\sigma = 1$ and $(z_1, z_2) \in \Omega_1$; therefore the active system continues being Σ_1 until the trajectory leaves region R_3 and goes to region R_2, instant in which there is a switching event to Σ_2. From Lemma 10 the trajectory has to return to a neighborhood of region R_3.
Region 4 (R_4). As $\sigma(t_0) = 1$, the active system is Σ_1. Then z_1 grows, while z_2 is constant. In the next instant t_1 there are two possibilities.

- Trajectory continues in region R_4. Due to $\sigma(t_1) = 1$ and $(z_1(t_1), z_2(t_1)) \notin \Omega_1$ the controller changes and the new active system is Σ_2. If with this new system the trajectory goes to region R_1, i.e., $(z_1(t_2), z_2(t_2)) \in \Omega_1$, it follows from Lemma 10 that trajectory remains in a neighborhood of R_4.

- Trajectory goes to region R_2. Due to $\sigma(t_1) = 1$ and $(z_1(t_1), z_2(t_1)) \notin \Omega_1$ the controller changes and the new active system is Σ_2. It follows from Lemma 10 that it remains in a neighborhood of R_4.

As it can be seen, both of them imply a switching event and it happens because $\sigma(t_i) = j$ ($j \in \{1, 2\}$) and $(x, s) \notin \Omega_j$. As long as the trajectory is in region R_4, the controller switches at every instant t_i. ■

Lemma 12. *System trajectories starting in R_3 or R_4 converge to a neighborhood of the optimal operating point asymptotically.*

Proof. **Region 3** (R_3). Trajectories arrive to this region by initial conditions or because they were driven from regions 1 or 2. For analysis, arriving by initial conditions or from R_1 is equivalent. Then, only two cases are considered: Σ_1 or Σ_2 is the active system.

1. Σ_1 is active: it continues active until the trajectory arrives to region R_2, time in which $(z_1(t_i), z_2(t_i)) \notin \Omega_1$.

2. Σ_2 is active: it continues active until the trajectory arrives to region R_1, time in which $(z_1(t_i), z_2(t_i)) \notin \Omega_2$.

In both cases all trajectories that start in R_3 are confined to live in its neighborhood (Lemma 11). The general behavior is as follows: the state is driven to a region (R_1 or R_2), for instance R_1 and, once trajectory has reached it, the active system changes to Σ_2. Then the trajectory evolves in the opposite direction and arrives to R_2, which produces a new switch to Σ_1. The pattern is repeated. For a very small diameter, the switching events occur almost in surfaces S_1 and S_2.

Since z_2 always grows in this region, and switching curves intersect at the optimal operating point (x^*, s^*), trajectories close region R_3 tend to an optimal-operating-point-neighborhood.

Region 4 (R_4). As in the previous region, there are two possibilities: Σ_1 or Σ_2 is the active system. However, the system behavior is completely different from the previous case; whichever the active system is, there is switching.

If trajectories stay near region R_4, convergence to the optimal operating point could be concluded by using similar arguments as before. Since z_2 always decreases in this region and switching curves intersect at the optimal operating point (x^*, s^*), trajectories close to region R_4 tend to an optimal-operating-point-neighborhood. ■

3.5 Controller Algorithm and Simulations

In this section, the proposed controller is implemented by using the numerical parameters shown in Table 3.1, which were selected to allow a comparison with the results of the ES strategy presented by Wang et al. (1999). Although we want to maximize $q\mu(\bar{s})\bar{x}$, while in Wang et al. (1999) $\bar{u}\bar{x}$ is maximized (i.e. the optimization problems are different), for $q = 1$ we have $\bar{Q} = \mu(\bar{s})\bar{x} = \bar{u}\bar{x}$, and the optimal points for both problems are identical. For simulations, the continuous time controller in Definition 7 is implemented as follows: There are two

Table 3.1: Selected parameters for simulation.

Parameter	Value
μ_0	1
K_s (Monod)	0.02
K_s (Haldane)	0.1
K_I (Haldane)	0.5
d	1
q	1
s_{in}	1
u_L	0
u_H	1.1
CI_1	$[x(0), s(0)] = [0.8, 0.05]$
CI_2	$[x(0), s(0)] = [1.05, 0.05]$
CI_3	$[x(0), s(0)] = [0.1, 0.05]$

different u values: u_L and u_H, and $u[0] = u_L$. At every iteration the sign of $Q[k] - Q[k-1]$ is calculated, and the input is updated considering Algorithm 1. To make it work correctly it is necessary to define $Q[-1] = 0$. Notice that this algorithm does not require measurement of neither x nor s, and only the measurement of Q is needed.

3.5.1 Simulations: ideal Case

First, we present the simulation results for a nominal plant, without considering any disturbance (noise or delays in the measurements). Due to results are quite similar for Monod and Haldane kinetics, here are presented Monod results. Figure 3.20 presents two trajectories in the state space, which represent the principal closed-loop behaviors.
For initial conditions CI_1, system trajectory changes its direction after it crosses one switching curve; the process is repeated, while the state converges to the optimal operating point. In the other case, with initial condition CI_2, trajectory goes to one switching curve and it experiments a sliding-mode-like behavior, because it slides to the optimal operating point along the switching curve $S(u_H)$. Whichever the initial condition is, trajectories converge to the optimal operating point.

Due to switched control experiment chattering, the reader must be wondering about the control signal. Output signal and control action are shown in Figure 3.21, for previous initial condi-

Data: $Q[k-1],\ Q[k],\ u[k]$

if $Q[k] - Q[k-1] \leq 0$ **then**

  if $u[k] == u_L$ **then**

    $u[k+1] = u_H$;

  else

    $u[k+1] = u_L$;

  end

else

  $u[k+1] = u[k]$;

end

Algorithm 1: Updating law for u, $k = 0, 1, 2, \ldots, n$.

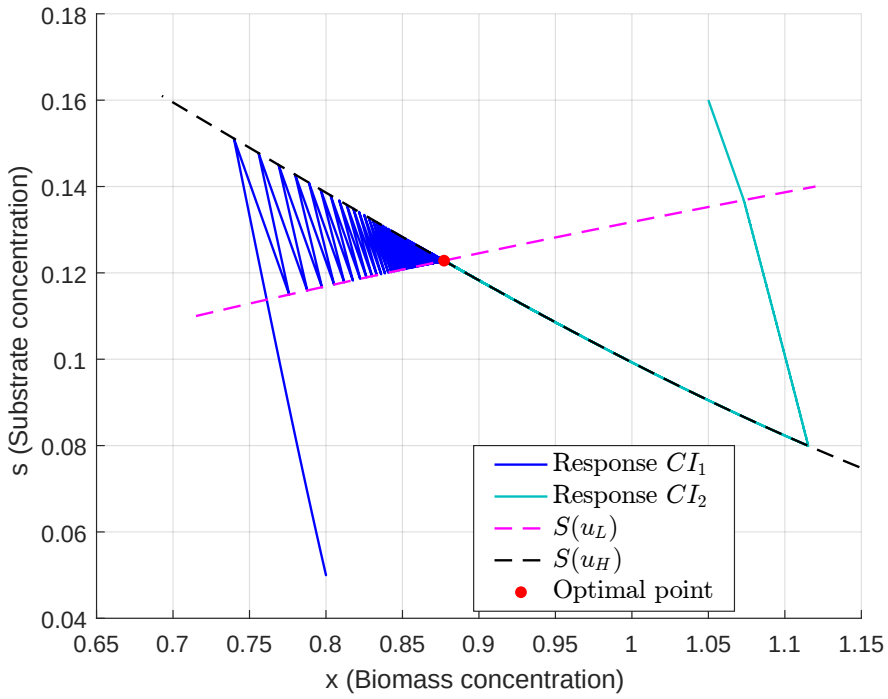

Figure 3.20: Fast Extremum Seeking: Monod kinetics with two initial conditions.

tions. It is appreciated that, effectively the input switches at every sampling time. However, bioreactors are slow systems and the switch can be applied with a big time partition, which is not dangerous for actuators.

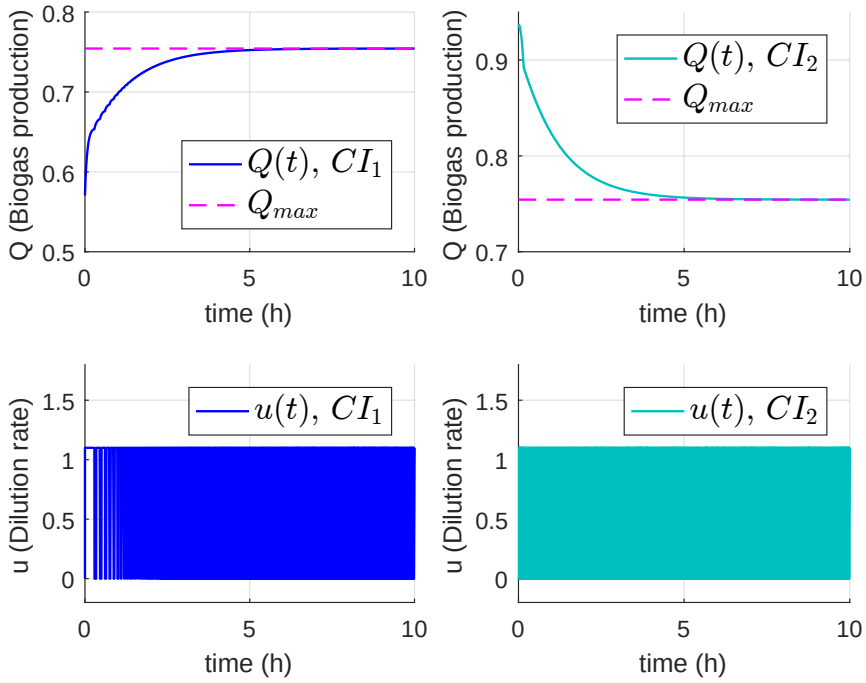

Figure 3.21: Fast Extremum Seeking: Monod kinetics with two initial conditions.

3.5.2 Comparisons: ideal case

Figure 3.22 present the closed-loop and open-loop control results, i.e., for open-loop the constant input which maximizes the biogas production u^* is assumed known and applied, while closed-loop behavior was obtained using Algorithm 1. It can be noticed that both the open-loop and closed-loop-settling-time are of the same magnitude order, independent of the tested initial conditions (approximately 7 h). It means that closed-loop performance is as good as knowing the optimal operating point.

On the other hand, there were made some simulations following the ideas presented in Wang et al. (1999); the selected parameters are shown in Table 3.2. Figure 3.23 shows system behavior with initial condition CI_1 for the system, and two initial conditions for the input. It is evident that system behavior is slower than our approach, because system achieve an stationary regiment approximately in 100 h with $u_0 = 0.6$ and 300 h for $u_0 = 0.55$. And as it can be seen, the convergence time is intimately related with the input initial condition. Additionally, in some simulations carried out with initial condition CI_2 system goes to washout.

It is clear that the difference in convergence is big enough to conclude that the proposed strategy is faster than traditional ES techniques. Needless to say, the control signal of traditional

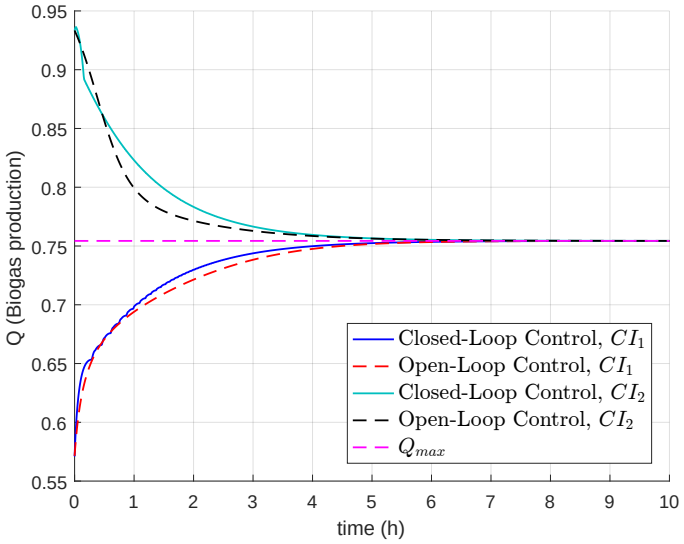

Figure 3.22: Closed-Loop and Open-Loop control: Monod kinetics with two initial conditions.

ES signal is smoother than switched control, which is better for the plant.

Table 3.2: Selected parameters for Wang et al. (1999) Extremum Seeking.

Parameter	Value
ω_h	0.04
ω	0.08
a	0.03
k	1.2

Besides the fastest convergence, it is important to remark that the proposed technique is independent of the reaction rate model, and it does not require knowing model parameters. It has only one parameter for tuning, and its value can be obtained by knowing an estimate of the upper bound of the reaction rate. Our approach works for every reaction rate satsfying Assumption 1 (Wang et al. (1999) approach needs a stabilizing feedback for non monotonic kinetics).

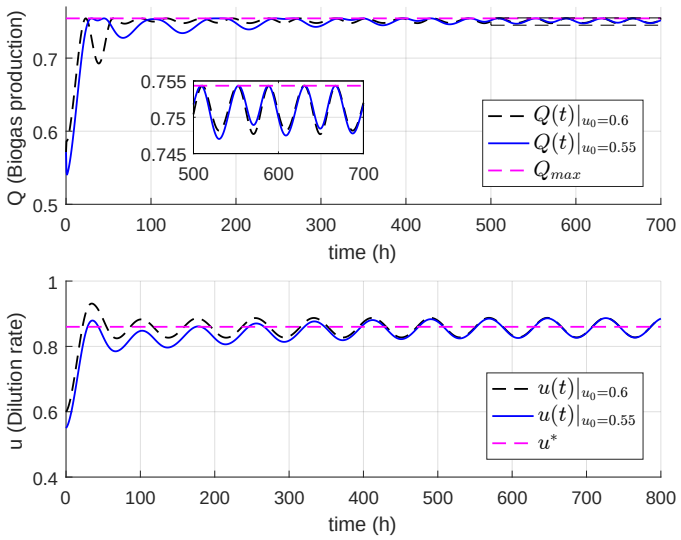

Figure 3.23: Closed-Loop and Open-Loop control: Monod kinetisc with two initial conditions.

3.5.3 Simulation: robustness test

In the previous subsection ideal simulations of closed loop performance were presented, i.e., it was assumed that perfect output measurement was available, parameters were static and that the controller was implemented in continuous time. However, for showing that closed loop stability is robust in realistic scenarios, it is necessary to present simulations considering the most common perturbations which occur in practice. For the following simulations nominal parameters are those in Table 3.1, but the same initial conditions (CI_3) are used for both reaction rate models.

The first test checked controller performance under noisy measurements which additionally are not available continuously. Noise was simulated by considering a Gaussian signal added to a low-frequency sinusoidal that multiplied the output; the combination produced a 2% maximum error in measurements. The system was simulated in continuous time, but the controller was implemented using a Zero-Order-Hold with sampling time of 1 minute.

Figures 3.24 and 3.25 show the system performance, with the described conditions. Once trajectories have reached optimal operating point vicinity, results for particular reaction rates can be analysed; in the Monod case, minimum biogas production is about 0.95 of its maximum value, while in the Haldane case it is around 0.98 of its maximum.

In both cases, the phase plane displays the effect of noise in trajectories, i.e., it produces premature or delayed switching events that guarantee only practical stability. However, these results show that the proposed controller is robust against noise in measurements and against

its discrete implementation. In fact, discretization helps to minimize noise impact because the controller only uses the difference between two measurements ($Q[k] - Q[k-1]$) and not the whole $Q(t)$ signal.

The second test checked the closed-loop response when s_{in} (inlet-substrate-concentration) changes with time. Two cases were considered: when the change in s_{in} is fast and when it is slow, with $s_{in} = 1 + 0.1\sin(\omega t)$ and $\omega = 0.25$ (slow variation) or $\omega = 200$ (fast variation). The simulation results are presented in Figs. 3.26 and 3.27.

In the same way as in the previous case (when only noise was considered), practical stability is achieved with fast and slow s_{in} variation. When s_{in} changes slowly, the output tries to follow the instantaneous optimal biogas production, i.e., the biogas production calculated using (2.6) or (2.9), respectively. On the other hand, when s_{in} changes fast, the output Q follows on the average of biogas production, which in this case corresponds with the nominal case, i.e., $\bar{Q}_{max}$ calculated with $s_{in} = 1$.

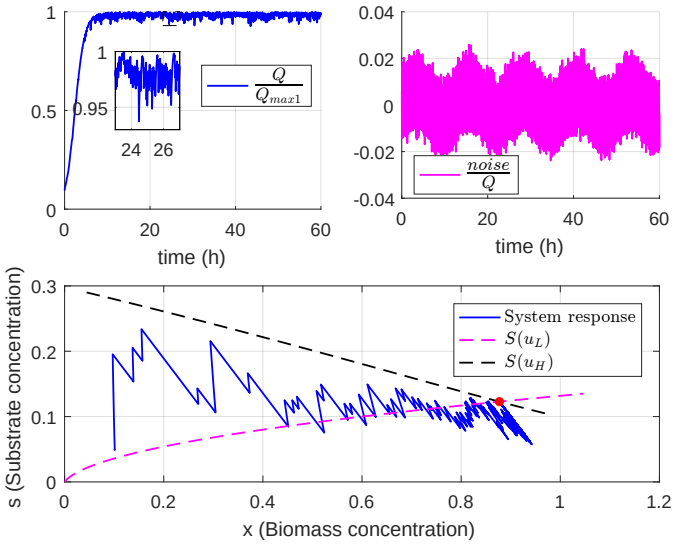

Figure 3.24: Monod reaction rate with CI_3 and noise in measurements.

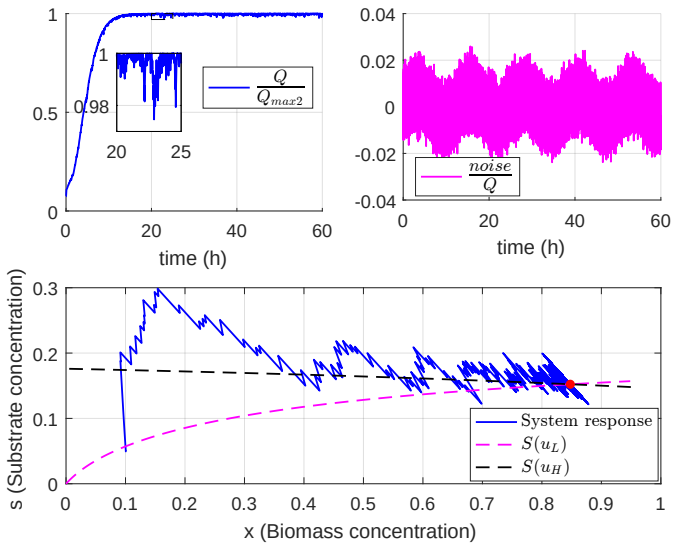

Figure 3.25: Haldane reaction rate with CI_3 and noise in measurements.

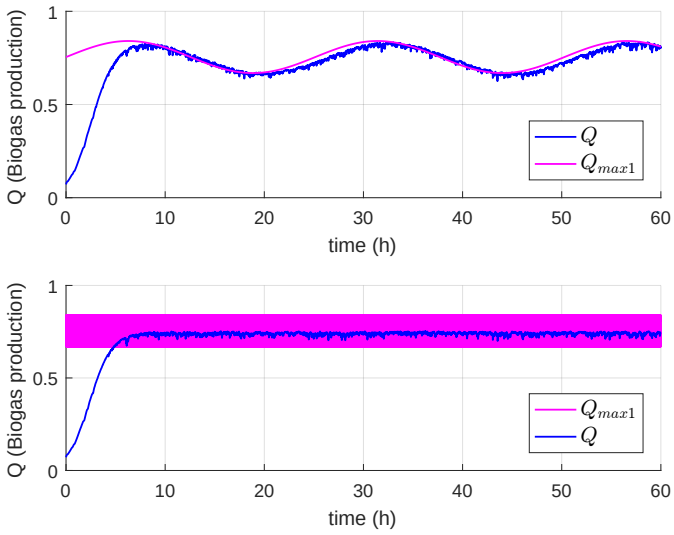

Figure 3.26: Monod reaction rate with CI_3, noise in measurements and time variant inlet-substrate-concentration $s_{in} = 1 + 0.1\sin(\omega t)$ (ω is 0.25 in the first plot and 200 in the second).

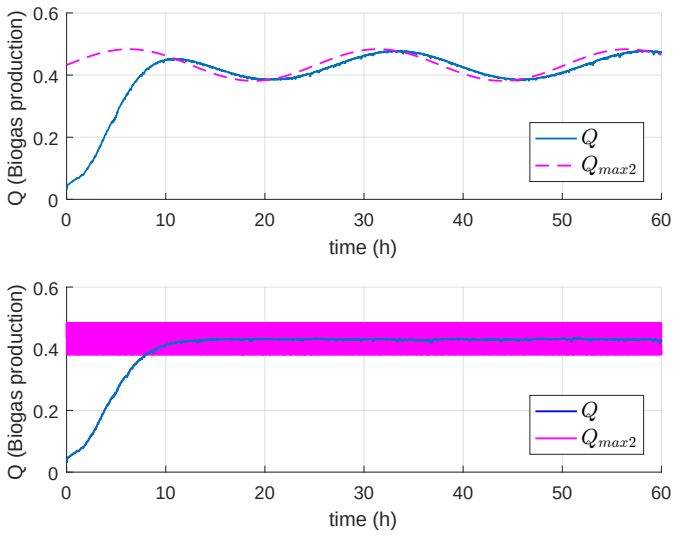

Figure 3.27: Haldane reaction rate with CI_3, noise in measurements and time variant inlet-substrate-concentration $s_{in} = 1 + 0.1\sin(\omega t)$ (ω is 0.25 in the first plot and 200 in the second).

Chapter 4

Partially Fixed-Bed Reactor: Controller Design

4.1 Testing the previous solution

In the previous chapter, a controller for the CSTR (when $\alpha = 1$) was designed, and before a new solution is proposed for the case $\alpha \in (0, 1)$ PFBR (Partially Fixed-Bed Reactor), it would be interesting to see what happens if Algorithm 1 is applied without any modification. The selected parameters are shown in Table 4.1; they are basically are the same as in the last simulations, but now $\alpha = 0.5$. Figures 4.1 and 4.2 display simulations for system (1.1) with Algorithm 1. Those plots show that system trajectories go to the intersection of $S(u_L)$ and $S(u_H)$, but in this case it does not correspond to the optimal operating point as before. To know the reason of this behavior, the intersection of $S(\bar{u})$ curves is analysed, and the definition of $\eta(x, s, u)$ as the time derivative of Q along system trajectories (1.1) is recalled.

$$\begin{aligned}
\eta(x,s,u) &\triangleq \frac{\mathrm{d}Q}{\mathrm{d}t} = \frac{\partial Q}{\partial x}\dot{x} + \frac{\partial Q}{\partial s}\dot{s}, \\
&= q\mu(s)\dot{x} + q\frac{\mathrm{d}\mu(s)}{\mathrm{d}s}x\dot{s}, \\
&= q\mu(s)(-\alpha u + \mu(s))x + q\frac{\mathrm{d}\mu(s)}{\mathrm{d}s}x\left(-d\mu(s)x + u(s_{in} - s)\right), \\
&= qx\left(\mu(s)(-\alpha u + \mu(s)) + \frac{\mathrm{d}\mu(s)}{\mathrm{d}s}\left(-d\mu(s)x + u(s_{in} - s)\right)\right). \qquad (4.1)
\end{aligned}$$

For a constant input $\bar{u}$, the curve $S(\bar{u}) = \{(x,\, s) \in \mathbb{R}^2_{\geq 0} | \eta(x, s, \bar{u}) = 0\}$ in the phase plane consists of the transient critical points for trajectories of the system (1.1) with the input $\bar{u}$, i.e., the points where Q has a local minimum, a maximum or an inflection point for that (constant) input. Making $\eta(x, s, u) = 0$ in (4.1), and ignoring the trivial solution $x = 0$,

$$\mu(s)(-\alpha u + \mu(s)) + \frac{\mathrm{d}\mu(s)}{\mathrm{d}s}\left(-d\mu(s)x + u(s_{in} - s)\right) = 0,$$

and solving for x it is obtained

$$x = \frac{u}{d}\left(\frac{s_{in}-s}{\mu(s)} - \frac{\alpha}{\frac{\mathrm{d}\mu(s)}{\mathrm{d}s}}\right) + \frac{\mu(s)}{d\frac{\mathrm{d}\mu(s)}{\mathrm{d}s}}. \tag{4.2}$$

Parameter	Value
α	0.5
μ_0	1
K_s (Monod)	0.02
K_s (Haldane)	0.1
K_I (Haldane)	0.5
d	1
q	1
s_{in}	1
u_L	0
u_H	2
CI_1	$[x(0), s(0)] = [1, 0.1]$
CI_2	$[x(0), s(0)] = [2, 0.25]$

Table 4.1: Selected parameters for simulation.

If two different values of u are taken: u_L (L: low) y u_H (H: high), there are two $S(\bar{u})$ curves

$$x_{u_L} = \frac{u_L}{d}\left(\frac{s_{in}-s}{\mu(s)} - \frac{\alpha}{\frac{\mathrm{d}\mu(s)}{\mathrm{d}s}}\right) + \frac{\mu(s)}{d\frac{\mathrm{d}\mu(s)}{\mathrm{d}s}},$$

$$x_{u_H} = \frac{u_H}{d}\left(\frac{s_{in}-s}{\mu(s)} - \frac{\alpha}{\frac{\mathrm{d}\mu(s)}{\mathrm{d}s}}\right) + \frac{\mu(s)}{d\frac{\mathrm{d}\mu(s)}{\mathrm{d}s}},$$

whose intersection can be checked making $x_{u_L} = x_{u_H}$,

$$\frac{u_L}{d}\left(\frac{s_{in}-s}{\mu(s)} - \frac{\alpha}{\frac{\mathrm{d}\mu(s)}{\mathrm{d}s}}\right) + \frac{\mu(s)}{d\frac{\mathrm{d}\mu(s)}{\mathrm{d}s}} = \frac{u_H}{d}\left(\frac{s_{in}-s}{\mu(s)} - \frac{\alpha}{\frac{\mathrm{d}\mu(s)}{\mathrm{d}s}}\right) + \frac{\mu(s)}{d\frac{\mathrm{d}\mu(s)}{\mathrm{d}s}},$$

$$\frac{u_H - u_L}{d}\left(\frac{s_{in}-s}{\mu(s)} - \frac{\alpha}{\frac{\mathrm{d}\mu(s)}{\mathrm{d}s}}\right) = 0,$$

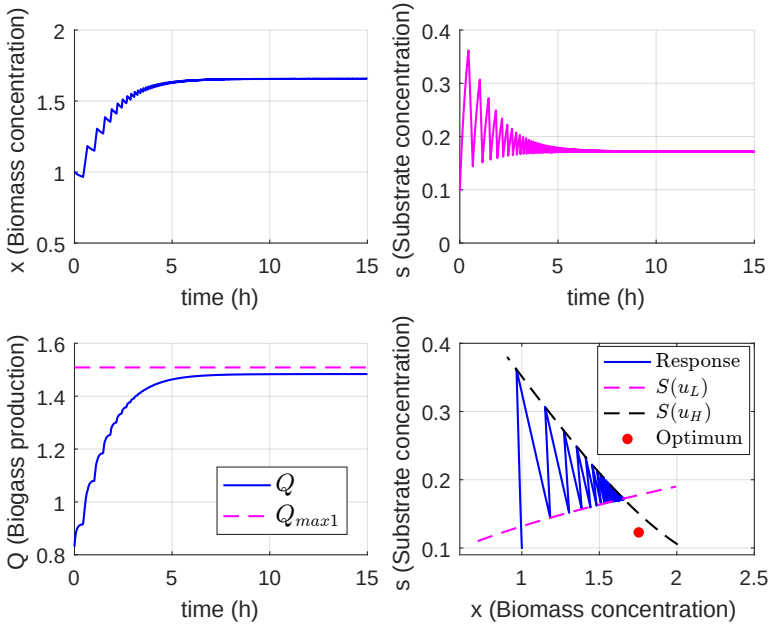

Figure 4.1: Closed loop: Monod reaction rate with CI_1.

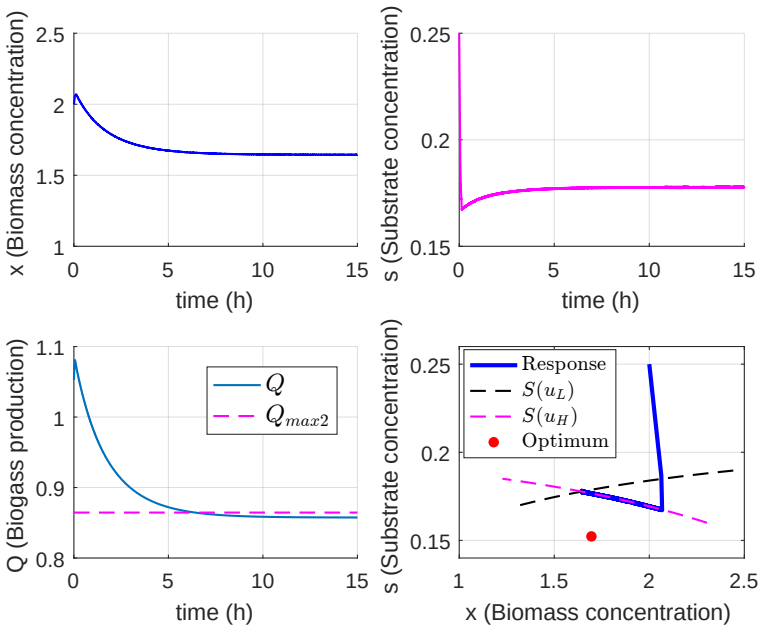

Figure 4.2: Closed loop: Haldane reaction rate with CI_2.

$$\frac{\mathrm{d}\mu(s)}{\mathrm{d}s}(s_{in}-s)-\alpha\mu(s)=0. \tag{4.3}$$

Replacing (4.3) in (4.2) it is obtained the following condition, which implies that it is an operating point:

$$x=\frac{s_{in}-s}{d\alpha}. \tag{4.4}$$

If (2.4) and (4.3) are compared, it is easily seen that they are different equations, which implies that the optimal operating point and the intersection of $S(\bar{u})$ curves are the same only when $\alpha=1$. Recall that the (optimal) solution to (2.4) does not depend on the parameter α, but the solution to (4.3) does. However, it is noticed that the values of u_L and u_H do not influence the intersection of the two $S(\bar{u})$ curves.

4.2 Designing new switching curves

The objective of this section is to obtain new switching curves to achieve the optimal operating point, in the same way that $S(\bar{u})$ curves work for the stirred tank reactor. A new output $R(x,s)$ is proposed such that its time derivative along system trajectories generates proper switching curves for maximizing Q.

For control purposes, it is defined the function $\eta_R(x,s,u)$ as the time derivative of R along the trajectories of system (1.1), i.e.,

$$\begin{aligned}
\eta_R(x,s,u) &\triangleq \frac{\partial R}{\partial x}\dot{x}+\frac{\partial R}{\partial s}\dot{s},\\
&= \frac{\partial R}{\partial x}(-\alpha u+\mu(s))x+\frac{\partial R}{\partial s}\left[-d\mu(s)x+u(s_{in}-s)\right],\\
&= q\mu(s)(-u+\mu(s))x+q\frac{\mathrm{d}\mu(s)}{\mathrm{d}s}x\left(-d\mu(s)x+u(s_{in}-s)\right),\\
&= u\left[-\alpha x\frac{\partial R}{\partial x}+\frac{\partial R}{\partial s}(s_{in}-s)\right]+\mu(s)x\frac{\partial R}{\partial x}-d\mu(s)x\frac{\partial R}{\partial s}.
\end{aligned} \tag{4.5}$$

For a constant input $\bar{u}$, the curve $S_R(\bar{u})=\{(x,\ s)\in\mathbb{R}^2_{\geq 0}|\eta_R(x,s,\bar{u})=0\}$ in the phase plane consists of the transient critical points of R for trajectories of system (1.1) with the input $\bar{u}$, i.e., the points where R has a local minimum, a maximum or an inflection point for that (constant) input.

Theorem 13. *Let*

$$R=q\mu(s)x^{\frac{1}{\alpha}}. \tag{4.6}$$

If (2.4) *has only one solution in the compact* $[0,s_{in}]$*, all curves* $S_R(\bar{u})$ *(generated with different* $\bar{u}$ *values) intersect at the optimal operating point.*

Proof. **Obtaining a proper output $R(x,s)$:**

It is necessary that all $S_R(\bar{u})$ intersect at the same point for all u, which implies that

$$\frac{\partial R}{\partial s}(s_{in}-s)-\alpha x\frac{\partial R}{\partial x}=0. \tag{4.7}$$

Furthermore, to satisfy $\eta_R(x,s,u)=0$ it is needed that:

$$\mu(s)x\frac{\partial R}{\partial x}-d\mu(s)x\frac{\partial R}{\partial s}=0. \tag{4.8}$$

From (4.8)

$$\frac{\partial R}{\partial x}=d\frac{\partial R}{\partial s}, \tag{4.9}$$

by using Equations (4.9) and (4.7) it follows,

$$\begin{aligned}\frac{\partial R}{\partial s}(s_{in}-s)-\alpha dx\frac{\partial R}{\partial s}&=0,\\ (s_{in}-s-\alpha dx)\frac{\partial R}{\partial s}&=0,\\ x&=\frac{s_{in}-s}{\alpha d}.\end{aligned} \tag{4.10}$$

Equation (4.10) implies that their intersection is an operating point, independently of $R(x,s)$. Because it must occur at the optimal operating point, equation (4.10) has to be satisfied, i.e.,

$$\frac{\mathrm{d}\mu(s)}{\mathrm{d}s}(s_{in}-s)-\mu(s)=0. \tag{4.11}$$

If (4.11) is multiplied by $\phi(x)$, it is obtained

$$\frac{\mathrm{d}\mu(s)}{\mathrm{d}s}(s_{in}-s)\phi(x)-\mu(s)\phi(x)=0. \tag{4.12}$$

One way to simultaneously satisfy (4.7) and (4.12) is proposing

$$\frac{\partial R}{\partial s}=\frac{\mathrm{d}\mu(s)}{\mathrm{d}s}\phi(x), \tag{4.13}$$

$$\alpha x\frac{\partial R}{\partial x}=\mu(s)\phi(x). \tag{4.14}$$

Then, by integrating (4.13) with respect to s it is found the next expression for R which has an unknown term ρ

$$R=\mu(s)\phi(x)+\rho(x).$$

Choosing $\rho(x) = 0$ and replacing the R expression in (4.14),

$$\alpha x \mu(s) \frac{\mathrm{d}\phi(x)}{\mathrm{d}x} = \mu(s)\phi(x),$$
$$\alpha x \frac{\mathrm{d}\phi(x)}{\mathrm{d}x} = \phi(x),$$

This differential equation can be solved separating variables and integrating

$$\int \frac{\mathrm{d}\left(\phi(x)\right)}{\phi(x)} = \frac{1}{\alpha} \int \frac{\mathrm{d}x}{x},$$
$$\ln(\phi(x)) = \frac{1}{\alpha} \ln(x) + C,$$
$$\ln(\phi(x)) = \ln\left(x^{\frac{1}{\alpha}}\right) + C,$$
$$\phi(x) = K x^{\frac{1}{\alpha}}.$$

Finally, choosing $K = q$, the expression for $R(x, s)$ is

$$R(x, s) = q\mu(s) x^{\frac{1}{\alpha}}. \tag{4.15}$$

Validation of $R(x, s)$:

$$\dot{R} = \frac{\partial R}{\partial x}\dot{x} + \frac{\partial R}{\partial s}\dot{s},$$

replacing (4.15) in (4.5), $S_R(x, s, u)$ curves are:

$$\frac{q}{\alpha}\mu(s)x^{\frac{1}{\alpha}}(-\alpha u + \mu(s)) + q\frac{\mathrm{d}\mu(s)}{\mathrm{d}s}x^{\frac{1}{\alpha}}\left(-d\mu(s)x + u(s_{in} - s)\right) = 0,$$
$$\frac{1}{\alpha}\mu(s)(-\alpha u + \mu(s)) + \frac{\mathrm{d}\mu(s)}{\mathrm{d}s}\left(-d\mu(s)x + u(s_{in} - s)\right) = 0,$$
$$u\left[-\mu(s) + \frac{\mathrm{d}\mu(s)}{\mathrm{d}s}(s_{in} - s)\right] + \frac{1}{\alpha}\mu(s)^2 - d\mu(s)x\frac{\mathrm{d}\mu(s)}{\mathrm{d}s} = 0, \tag{4.16}$$

at the intersection, the previous relation has to be satisfied for any u, which implies that

$$\frac{\mathrm{d}\mu(s)}{\mathrm{d}s}(s_{in} - s) - \mu(s) = 0, \tag{4.17}$$
$$\frac{1}{\alpha}\mu(s)^2 - d\mu(s)x\frac{\mathrm{d}\mu(s)}{\mathrm{d}s} = 0. \tag{4.18}$$

Combining equations (4.17) and (4.18), it is recovered the stationary condition

$$x = \frac{s_{in} - s}{d\alpha}. \tag{4.19}$$

Since (2.2) and (2.4) are satisfied, it is concluded that $S_R(x, s, u)$ curves, generated with different u values intersect at the optimal operating point. ■

In particular, if Monod and Haldane reaction rates are considered, for some set of parameters, and using different u values, their asociated $S_R(\bar{u})$ curves are shown in Figure (4.3). And, as it was demonstrated, in Theorem 13, all of them intersect at the optimal operating point (x^*, s^*).

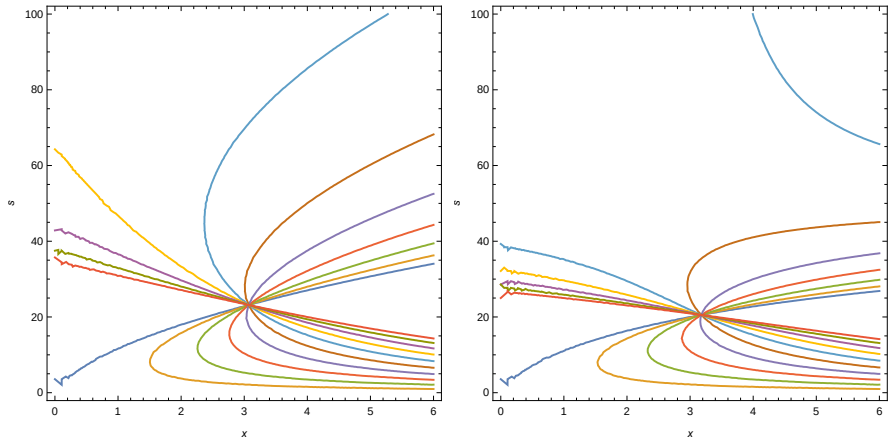

(a) Monod reaction rate. **(b)** Haldane reaction rate.

Figure 4.3: $S(\bar{u})$ curves for both reaction rates.

4.3 Phase plane with complete dynamics

Taking the same restriction as in the CSTR, $u_L = 0$ and $u_H > \frac{\mu_{max}}{\alpha}$, which define the dynamics of Σ_1 and Σ_2 the phase planes presented in Figure 4.4 are generated. Those plots show that switching curves intersect at the optimal operating point, and that it can be reached with a proper switching algorithm.

4.4 Fast Extremum Seeking Controller

As we obtained the switching curves $S_R(\bar{u})$, the controller definition is almost the same as Definition 7, because it is only needed to define $S_1 = S_R(u_L)$ and $S_2 = S_R(u_H)$.

Definition 14. ***(Controller)*** *Define* $\Omega_1 = \{\eta_R(x, s, u_L) > 0\}$, $\Omega_2 = \{\eta_R(x, s, u_H) > 0$, *(for non-monotonic* $\mu(s)$, $s < s_c)\}$ *and introduce the discrete state* σ, *whose role is to specify, at each time instant* $t \geq 0$, *the index* $\sigma \in \{1, 2\}$ *of the active system. Let* $\sigma(t_0) = 1$ *and define* $\pi = \{t_i\}_{i=0}^{\infty}$ *as a partition of* $[0, \infty)$, *with a very small diameter* $\mathrm{diam}(\pi) \triangleq \sup_{i\in\{1,2,\ldots\}}(t_i - t_{i-1})$.

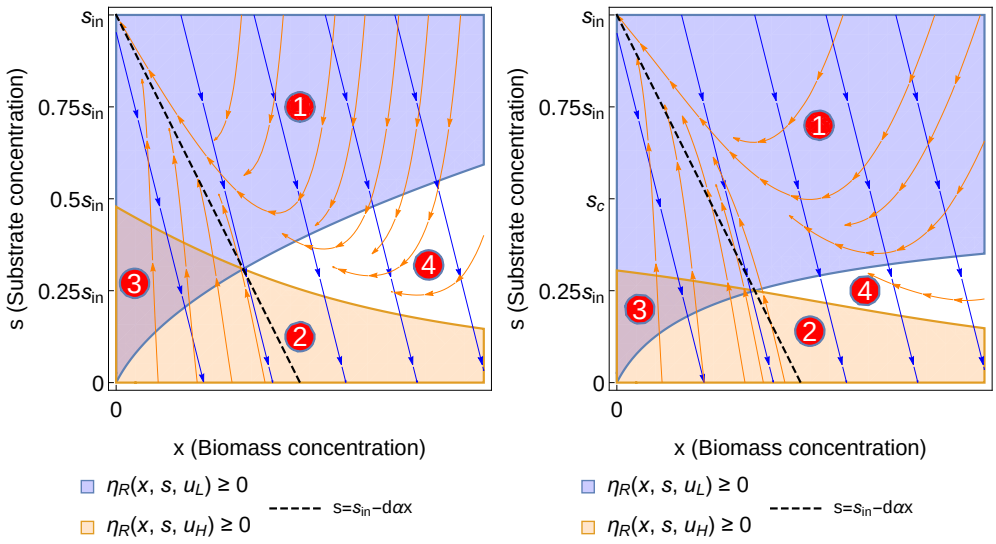

(a) Monod reaction rate.

(b) Haldane reaction rate.

Figure 4.4: Phase portrait for complete dynamics with $u_L = 0$ and $u_H > \mu_{\max}$ $(0 < \alpha < 1)$. The operating points set is shown in black.

At the beginning, let the system evolve as Σ_1 *in the interval* $[t_0, t_1]$*. Then, for each* $t_i \geq t_1$*, if* $\sigma(t_{i-1}) = j \in \{1, 2\}$ *and* $(x(t_i), s(t_i)) \in \Omega_j$*, make* $\sigma(t_i) = j$*. On the other hand, if* $\sigma(t_{i-1}) = 1$ *but* $(x(t_i), s(t_i)) \notin \Omega_1$*, let* $\sigma(t_i) = 2$*. In the same way, if* $\sigma(t_{i-1}) = 2$ *but* $(x(t_i), s(t_i)) \notin \Omega_2$*, let* $\sigma(t_i) = 1$*. It is said that a switching event occurs when* σ *changes its value.*

The closed loop trajectories, generated with this algorithm, can be understood as the $\pi -$ *solutions of 1.1 by defining recursively the applied input (*u_L *or* u_H*).* △

The previous definition expresses the following system behavior: at the beginning it is applied u_L as an initial condition. The signum of $\frac{\mathrm{d}R}{\mathrm{d}t}$ is checked at every instant t_i and when $\frac{\mathrm{d}R}{\mathrm{d}t}|_{t=t_i} \leq 0$, the input value u is switched. It means that it is desired to search the optimal operating point by making R grow as much as possible, or by making R decrease in a proper way. The properties of Controller in Definition 14 in the nominal case are given in the Theorem 15.

Theorem 15. *Assume that* $\mu(s)$ *is at least once differentiable and it satisfies one of the following statements:*

- $\mu(s)$ *is concave monotonic increasing.*

- $\mu(s)$ *is convex monotonic increasing.*
- $\mu(s)$ *has only one maximum in* $s_c \in (0, s_{in})$*, it is concave monotonic increasing in* $[0, s_c]$*, and monotonic decreasing in* $[s_c, s_{in}]$.

Consider the Controller in Definition 14, system (3.1) and consider that $\text{sign}(\frac{\mathrm{d}R}{\mathrm{d}t})$ *is available for measurement. Given a neighborhood of the optimal operating point, there exists* π^* *such that if* $\text{diam}(\pi) < \text{diam}(\pi^*)$ *trajectories achieve it asymptotically for any initial condition* $(x(0),\, s(0)) \in \Omega$ $(x(0) \neq 0)$.

Proof. The proof is basically the same as the proof of Theorem 8 with some changes. Define the following regions: $R_1 = \Omega_1 \cap \Omega_2^c$, $R_2 = \Omega_1^c \cap \Omega_2$, $R_3 = \Omega_1 \cap \Omega_2$ and $R_4 = \Omega_1^c \cap \Omega_2^c$. The proof is based on the following statements.

- Theorem 13: all $S_R(\bar{u})$ curves intersect at the optimal operating point.
- Lemma 16: Assume that $\mu(s)$ is at least once differentiable and it satisfies one of the following statements:
  - $\mu(s)$ is concave monotonic increasing.
  - $\mu(s)$ is convex monotonic increasing.
  - $\mu(s)$ has only one maximum in $s_c \in (0, s_{in})$, it is concave monotonic increasing in $[0, s_c]$, and monotonic decreasing in $[s_c, s_{in}]$.

  $S_1 = S_R(u_L)$ and $S_2 = S_R(u_H)$ divide the state space in four regions R_1, R_2, R_3 and R_4, which are oriented clockwise $R_1 - R_4 - R_2 - R_3$ as shown in Figure 4.4.
- Lemma 17: system trajectories starting in R_1 or R_2 reach R_3 or R_4 in finite time.
- Lemma 18: system trajectories starting in R_3 or R_4 remain in a neighborhood of R_3 or R_4, respectively.
- Lemma 19: system trajectories starting in R_3 or R_4 converge to a neighborhood of the optimal operating point asymptotically.

■

Lemma 16. *Assume that $\mu(s)$ is at least once differentiable and it satisfies one of the following statements:*

- *$\mu(s)$ is concave monotonic increasing.*
- *$\mu(s)$ is convex monotonic increasing.*
- *$\mu(s)$ has only one maximum in $s_c \in (0, s_{in})$, it is concave monotonic increasing in $[0, s_c]$, and monotonic decreasing in $[s_c, s_{in}]$.*

$S_1 = S_R(u_L)$ and $S_2 = S_R(u_H)$ divide the state space in four regions R_1, R_2, R_3 and R_4, which are oriented clockwise $R_1 - R_4 - R_2 - R_3$ as shown in Figure 4.4.

Proof. The proof is exactly the same as the proof of Lemma 9, but taking the following expressions for the switching curves:

$$S_1 : \left\{ x = \frac{\mu(s)}{d\alpha\mu'(s)} \right. . \tag{4.20}$$

$$S_2 : \left\{ \frac{u_H}{d} \left(\frac{s_{in} - s}{\mu(s)} - \frac{1}{\mu'(s)} \right) + \frac{\mu(s)}{d\mu'(s)} \right. . \tag{4.21}$$

■

Lemma 17. *System trajectories starting in R_1 or R_2 reach R_3 or R_4 in finite time.*

Proof. The following coordinate change is introduced, in order to make the analysis easier

$$z_1 = x, \tag{4.22}$$

$$z_2 = dx + s. \tag{4.23}$$

Bioreactor dynamics (1.1) in the new coordinates has the following representation.

$$\dot{z}_1 = -\left(\alpha u - \mu(z_2 - dz_1)\right) z_1, \tag{4.24}$$

$$\dot{z}_2 = -\left(z_2 - s_{in} - d(1-\alpha)z_1\right) u. \tag{4.25}$$

and therefore, Σ_1 and Σ_2 are as follows

$$\Sigma_1 : \begin{cases} \dot{z}_1 = \mu(z_2 - dz_1)z_1, \\ \dot{z}_2 = 0. \end{cases} \tag{4.26}$$

For Σ_1, z_1 increases and z_2 is maintained constant.

$$\Sigma_2 : \begin{cases} \dot{z}_1 = -\left(\alpha u_H - \mu(z_2 - dz_1)\right) z_1, \\ \dot{z}_2 = -\left(z_2 - s_{in} - d(1-\alpha)z_1\right) u_H. \end{cases} \tag{4.27}$$

For Σ_2, z_1 decreases and z_2 has three different options. $z_2 = s_{in} + d(1-\alpha)z_1$ is the equilibria set obtained from (2.2) in new coordinates.

1. If $z_2 < s_{in} + d(1-\alpha)z_1$, z_2 increases.
2. If $z_2 = s_{in} + d(1-\alpha)z_1$, z_2 is maintainded constant at least an instant.
3. If $z_2 > s_{in} + d(1-\alpha)z_1$, z_2 decreases.

For completeness of the proof, it is necessary to recover the form of previous axes.

- Mapping $x = 0$ (axis s):

$$\begin{aligned} z_1 &= 0, \\ z_2 &= s. \end{aligned}$$

  Which implies that the s and z_2 axes are coincident.

- Mapping $s = 0$ (axis x):

$$z_2 = dz_1$$

  Which implies that x axis is a line with slope d that crosses the origin.

- Additionally, let z_1^* and z_2^* be the optimal operating values in new coordinates.

Phase planes presented in Figure 4.4 in new coordinates, are presented in Figure 4.5, in order to graphically understand the coordinates change. It can be seen that the state space is divided in

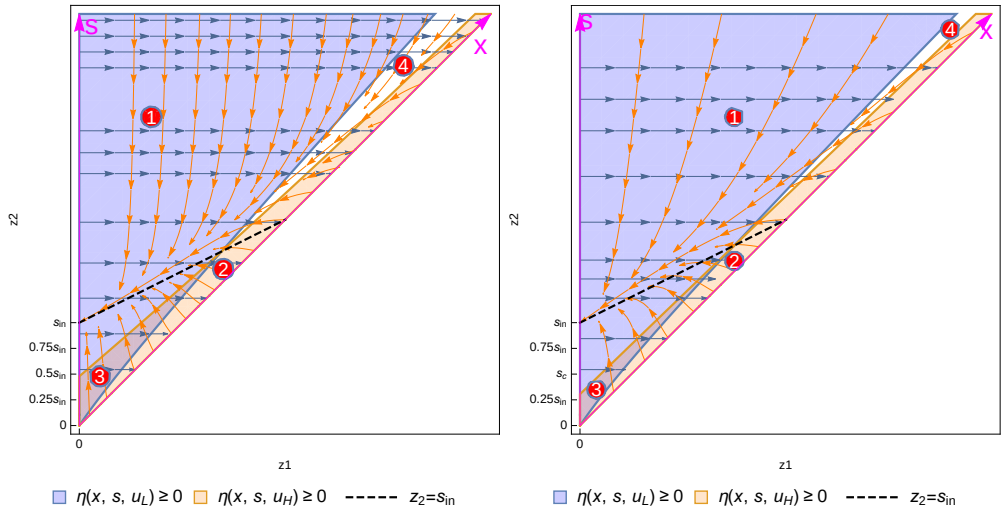

(a) Monod reaction rate.

(b) Haldane reaction rate.

Figure 4.5: Phase portrait with $u_L = 0$ and $u_H > \mu_{\max}$ in z coordinates.

four operating regions, independent of the reaction rate. To ensure convergence, it is necessary to analyse all of them, considering initial conditions inside each one and looking at how trajectories behave. Also, it is necessary to remember that $u(t_0) = u_L$, and that π is sufficiently small that trajectories move very little during each interval $[t_{i-1}, t_i]$ $i \in \{1, 2, \dots\}$.

Region 1 (R_1). It was stated that $\sigma(t_0) = 1$, therefore the active system is Σ_1 and $(z_1, z_2) \in \Omega_1$, which implies that z_1 grows while z_2 remains constant. Then, there are three possibilities:

1. If $z_2 \leq z_2^*$, trajectories go to region R_3 without a switching event, then the active system continues being Σ_1. If the trajectory is close to the optimal state the trajectory may quickly pass region R_3 and end at t_i in R_2 to region R_2 with a switching event to Σ_2.

2. If $z_2 = z_2^*$, trajectories arrive to the optimal operating point with a switching event (the switch can occur exactly at the optimal operating point or after passing it, as system could go to region R_2 due to the partition π), then the active system changes to Σ_2.

3. If $z_2 \geq z_2^*$, trajectories could go to R_4 with a switching event (the switch can occur exactly at the surface S_1 or after passing it, due to the partition π). If trajectory is close

to the optimal state it could end in region R_2. Whichever the case is, the active system changes to Σ_2.

Region 2 (R_2). It was said that $\sigma(t_0) = 1$, then the active system is Σ_1, but $(z_1, z_2) \notin \Omega_1$. This fact produces an initial switching event to system Σ_2. When Σ_2 is the active system, z_1 decreases, and there are three cases:

1. Trajectories could go to region R_3 without a switching event, then the active system continues being Σ_2. If trajectory is close to the optimal state, it could end in region R_1 with a switching event to Σ_1.

2. Trajectories arrive to the optimal operating point with a switching event (the switch can occur exactly at the optimal operating point or after passing it, as system could go to region R_1 due to the partition π), then the active system changes to Σ_1.

3. Trajectories could go to R_4 with a switching event (the switch can occur exactly at the surface S_2 or after passing it, due to the partition π). If trajectory is close to the optimal state it could end in region R_1. Whichever the case is, the active system changes to Σ_2.

Finite time convergence can be obtained from the fact that Σ_1 and Σ_2 have different asymptotically stable equilibrium points (they are not the optimal operating point). Since trajectories need to cross switching surfaces to achieve those equilibria, it is concluded that trajectories starting at $(z_1, z_2) \in R_1 \cup R_2$ reach $R_3 \cup R_4$ in finite time. ■

Lemma 18. *System trajectories starting in R_3 or R_4 remain in neighborhood of R_3 or R_4, respectively.*

Proof. **Region 3** (R_3). As $\sigma(t_0) = 1$, the active system is Σ_1. Then z_1 grows, while z_2 is constant. $\sigma = 1$ and $(z_1, z_2) \in \Omega_1$; therefore the active system continues being Σ_1 until the trajectory leaves region R_3 and goes to region R_2, instant in which there is a switching event to Σ_2. From Lemma 17 the trajectory has to return to a neighborhood of region R_3.
Region 4 (R_4). As $\sigma(t_0) = 1$, the active system is Σ_1. Then z_1 grows, while z_2 is constant. In the next instant t_1 there are two possibilities.

- Trajectory continues in region R_4. Due to $\sigma(t_1) = 1$ and $(z_1(t_1), z_2(t_1)) \notin \Omega_1$ the controller changes and the new active system is Σ_2. If with this new system the trajectory goes to region R_1, i.e., $(z_1(t_2), z_2(t_2)) \in \Omega_1$, it follows from Lemma 17 that trajectory remains in a neighborhood of R_4.

- Trajectory goes to region R_2. Due to $\sigma(t_1) = 1$ and $(z_1(t_1), z_2(t_1)) \notin \Omega_1$ the controller changes and the new active system is Σ_2. It follows from Lemma 17 that it remains in a neighborhood of R_4.

As it can be seen, both of them imply a switching event and it happens because $\sigma(t_i) = j$ ($j \in \{1, 2\}$) and $(x, s) \notin \Omega_j$. As long as the trajectory is in region R_4, controller switches at every instant t_i. ■

Lemma 19. *System trajectories starting in R_3 or R_4 converge to a neighborhood of the optimal operating point asymptotically.*

Proof. **Region 3** (R_3). Trajectories arrive to this region by initial conditions or because they were driven from regions 1 or 2. For analysis, arriving by initial conditions or from R_1 is equivalent. Then, only two cases are considered: Σ_1 or Σ_2 is the active system.

1. Σ_1 is active: it continues active until the trajectory arrives to region R_2, time in which $(z_1(t_i), z_2(t_i)) \notin \Omega_1$.

2. Σ_2 is active: it continues active until the trajectory arrives to region R_1, time in which $(z_1(t_i), z_2(t_i)) \notin \Omega_2$.

In both cases all trajectories that start in R_3 are confined to live in its neighborhood (Lemma 18). The general behavior is as follows: the state is driven to a region (R_1 or R_2), for instance R_1 and, once trajectory has reached it, the active system changes to Σ_2. Then the trajectory evolves in the opposite direction and arrives to R_2, which produces a new switch to Σ_1. The pattern is repeated. For a very small diameter, the switching events occur almost in surfaces S_1 and S_2.

Since z_2 always grows in this region (in R_3 $z_2 < s_{in} + d(1-\alpha)z_1$), and switching curves intersect at the optimal operating point (z_1^*, z_2^*), trajectories close region R_3 tend to an optimal-operating-point-neighborhood.

Region 4 (R_4). As in the previous region, there are two possibilities: Σ_1 or Σ_2 is the active system. However, the system behavior is completely different from the previous case; whichever the active system is, there is switching.

If trajectories stay near region R_4, convergence to the optimal operating point could be concluded by using similar arguments as before. Since z_2 always decreases in this region (in R_3 $z_2 > s_{in} + d(1-\alpha)z_1$) and switching curves intersect at the optimal operating point (z_1^*, z_2^*), trajectories close to region R_4 tend to an optimal-operating-point-neighborhood. ■

4.5 Controller Algorithm and Simulations

In this section, the proposed controller is implemented for both possible reaction rates by using the numerical parameters shown in Table 4.1. For simulations, the continuous time controller in Definition 14 is implemented as follows: There are two different u values: u_L and u_H, and $u[0] = u_L$. At every iteration the sign of $R[k] - R[k-1]$ is calculated, and the input is updated considering Algorithm 2. To make it work correctly it is necessary to define $R[-1] = 0$. In this case, additional information about the system is needed; R is calculated as $R = q\mu(s)x^{\frac{1}{\alpha}} = Qx^{\frac{1-\alpha}{\alpha}}$, which implies on the one hand that α is known, and on the other hand that Q and x are measured.

4.5.1 Simulations: ideal case

As before, first we present the simulation results for a nominal plant, without considering any disturbance (noise or delays in the measurements). Also, there are presented only Monod results because for Haldane it is obtained a similar response. Figure 4.6 presents two trajectories in the state space, which represent the principal closed-loop behaviors.
The conclusions are the same as in the CSTR. For initial conditions CI_1, system trajectory changes its direction after it crosses one switching curve; the process is repeated, while the state converges to the optimal operating point. In the other case, with initial condition CI_2, trajectory goes to one switching curve and it experiments a sliding-mode-like behavior, because it slides to the optimal operating point along the switching curve $S(u_H)$. Whichever the initial condition is, trajectories converge to the optimal operating point.

Data: $R[k-1],\ R[k],\ u[k]$

if $R[k] - R[k-1] \leq 0$ **then**

  if $u[k] == u_L$ **then**

    $u[k+1] = u_H$;

  else

    $u[k+1] = u_L$;

  end

else

  $u[k+1] = u[k]$;

end

Algorithm 2: Updating law for u, $k = 0, 1, 2, \ldots, n$.

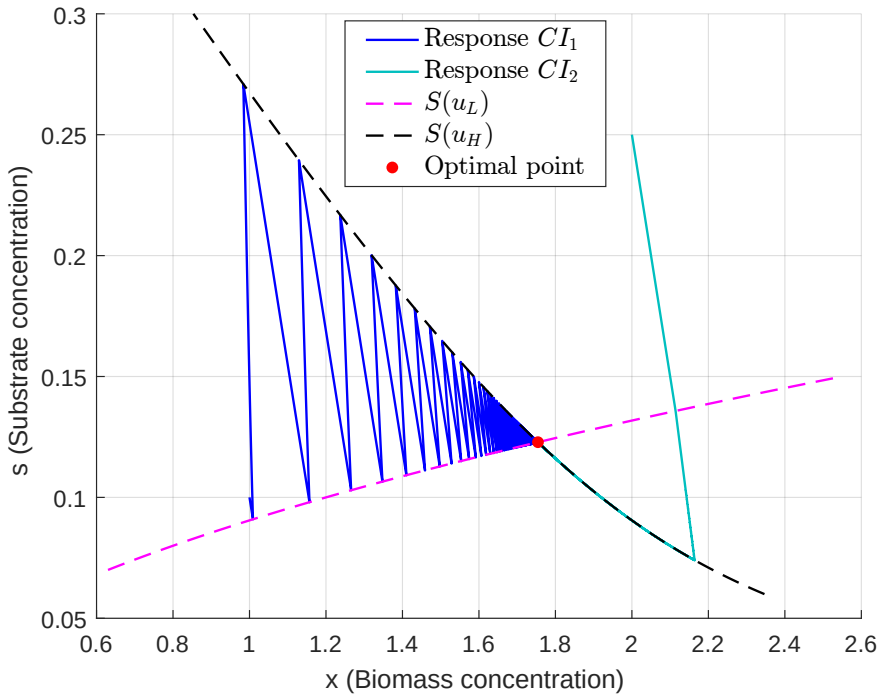

Figure 4.6: Fast Extremum Seeking: Monod kinetics with two initial conditions.

Output signal and control action are shown in Figure 4.7. It is appreciated that the input switches at every sampling time. However, bioreactors are slow systems and the switch can

be applied with a big time partition, which is not dangerous for actuators.

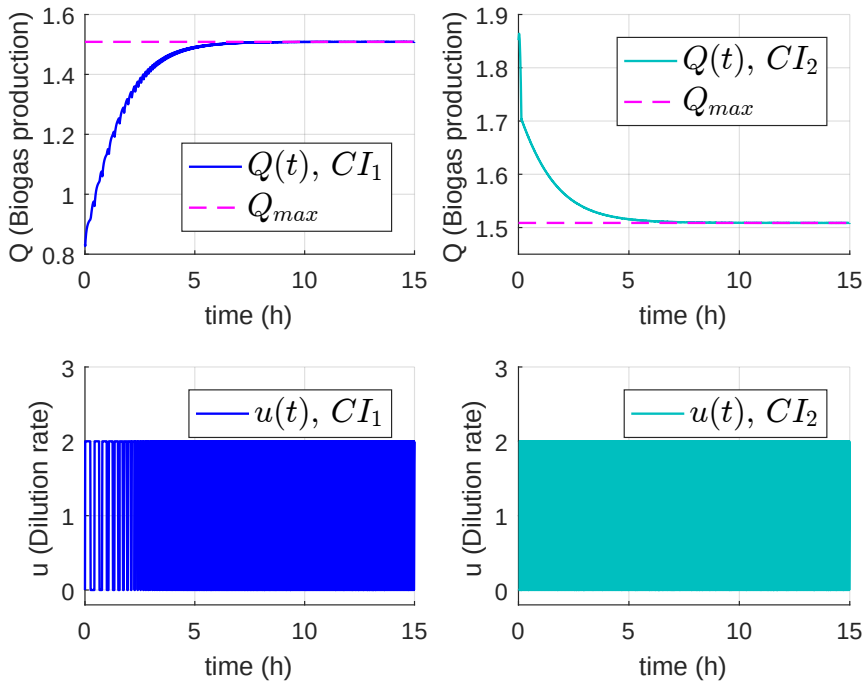

Figure 4.7: Fast Extremum Seeking: Monod kinetics with two initial conditions.

4.5.2 Comparisons: ideal case

Figure 4.8 present closed-loop and open-loop control results, i.e., for open-loop the constant input which maximizes the biogas production u^* is assumed known and applied, while closed-loop behavior was obtained using Algorithm 2. It can be noticed that both the open-loop and closed-loop-settling-time are of the same magnitude order, independent of the tested initial conditions (approximately 10 h). It means that closed-loop performance is as good as knowing the optimal operating point.

On the other hand, there were made some simulations following the ideas pesented in Wang et al. (1999); the selected parameters are shown in Table 4.2. Figure 4.9 shows system behavior with initial condition CI_1 for the system, and two initial conditions for the input. It is evident that system behavior is slower than our approach, because system achieve an stationary regiment approximately in 3000 h. In some simulations carried out with initial condition CI_2 system goes to washout.

It is clear that the difference in convergence is big enough to conclude that the proposed strat-

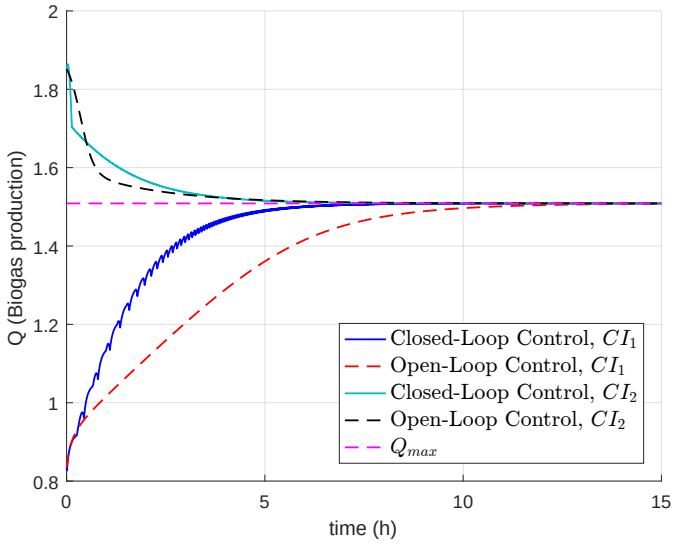

Figure 4.8: Closed-Loop and Open-Loop control: Monod kinetisc with two initial conditions.

egy is faster than traditional ES techniques. Needless to say, the control signal of traditional ES signal is smoother than switched control, which is better for the plant.

Table 4.2: Selected parameters for Wang et al. (1999) Extremum Seeking.

Parameter	Value
ω_h	0.04
ω	0.08
a	0.03
k	1.2

Besides the fastest convergence, it is important to remark that the proposed technique is independent of the reaction rate model, and it does not require knowing model parameters. It has only one parameter for tuning, and its value can be obtained by knowing an estimate of the upper bound of the reaction rate. Our approach works for every reaction rate satsfying Assumption 1 (Wang et al. (1999) approach needs a stabilizing feedback for non monotonic kinetics).

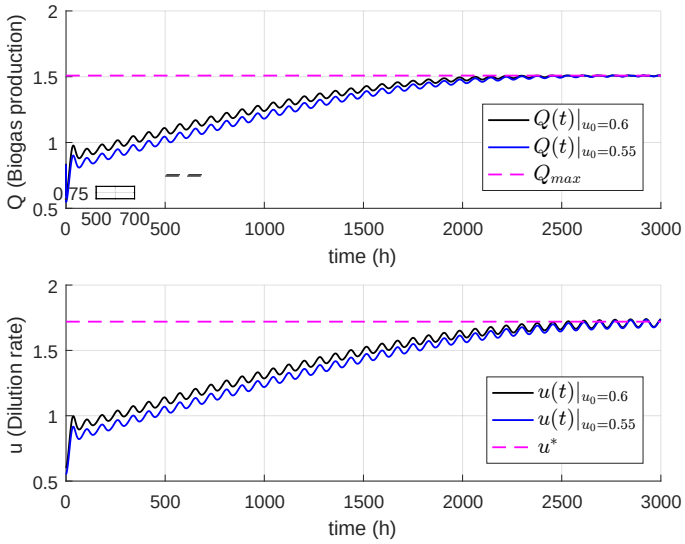

Figure 4.9: Closed-Loop and Open-Loop control: Monod kinetisc with two initial conditions.

4.5.3 Simulation: robustness test

In the previous subsection ideal simulations of closed loop performance were presented, i.e., it was assumed that perfect output measurement was available, parameters were static and that the controller was implemented in continuous time. However, for showing that closed loop stability is robust in realistic scenarios, it is necessary to present simulations considering the most common perturbations which occur in practice.

The first test checked controller performance under noisy measurements which additionally are not available continuously. Noise was simulated by considering a Gaussian signal added to a low-frequency sinusoidal that multiplied the output; the combination produced a 2% maximum error in measurements. The system was simulated in continuous time, but the controller was implemented using a Zero-Order-Hold with a sampling time of 1 minute.

Figures 4.10 and 4.11 show system performance with the described conditions. Once trajectories have reached the vicinity of optimal operating point, results for particular reaction rates can be analised; in the Monod case, minimum biogas production is about 0.90 of its maximum value, while in the Haldane case it is around 0.96 of its maximum.

In both cases, phase plane displays the effect of noise in trajectories, i.e., it produces premature or delayed switching events that guaranteed only practical stability. However, these results show that the proposed controller is robust against noise in measurements and against its discrete implementation. In fact, discretization helps to minimize noise impact because the controller only uses the difference between two measurements ($R[k] - R[k-1]$) and not the

whole $R(t)$ signal.

The second test checked the closed-loop response when s_{in} (inlet-substrate-concentration) changes with time. Two cases were considered: when the change in s_{in} is fast and when it is slow, with $s_{in} = 1 + 0.1\sin(\omega t)$ and $\omega = 0.25$ (slow variation) or $\omega = 200$ (fast variation). The simulation results are presented in Figs. 4.12 and 4.13.

In the same way as in the previous case (when only noise was considered), practical stability is achieved with fast and slow s_{in} variation. When s_{in} changes slowly, the output tries to follow the instantaneous optimal biogas production, i.e., the biogas production calculated using (2.6) or (2.9), respectively. On the other hand, when s_{in} changes fast, the output Q reaches the average of biogas production, which in this case corresponds with the nominal case, i.e., $\bar{Q}_{max}$ calculated with $s_{in} = 1$.

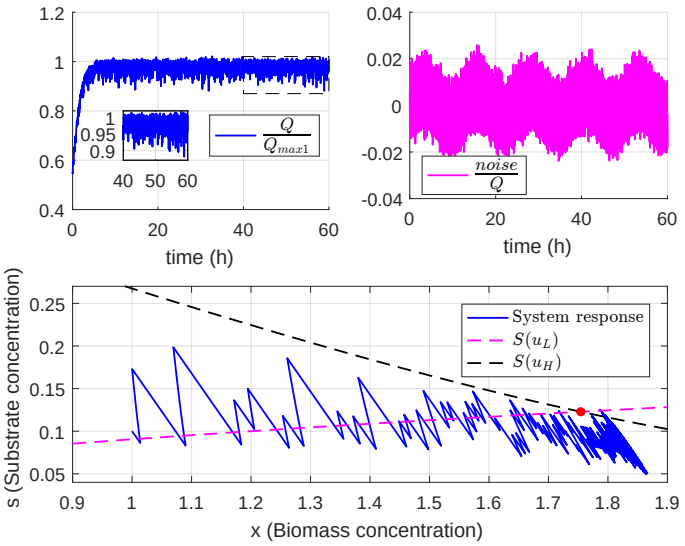

Figure 4.10: Monod reaction rate with CI_3 and noise in measurements.

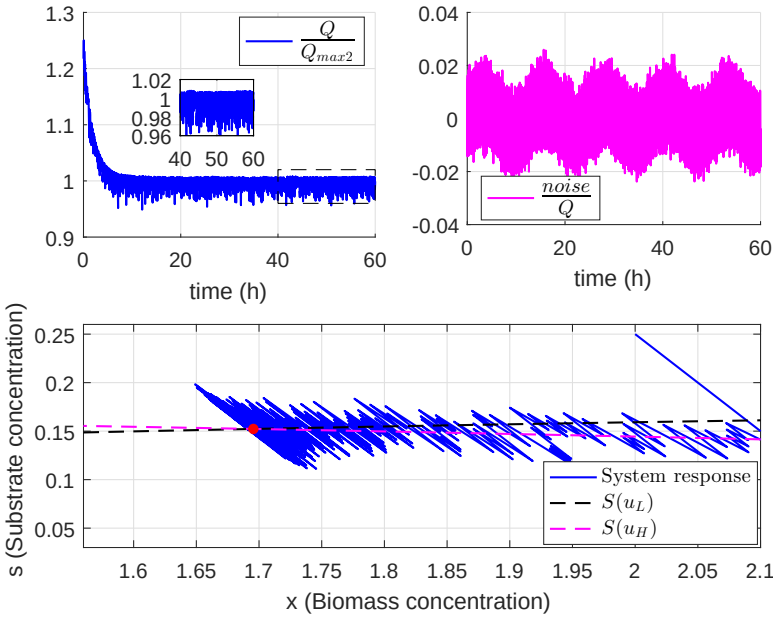

Figure 4.11: Haldane reaction rate with CI_3 and noise in measurements.

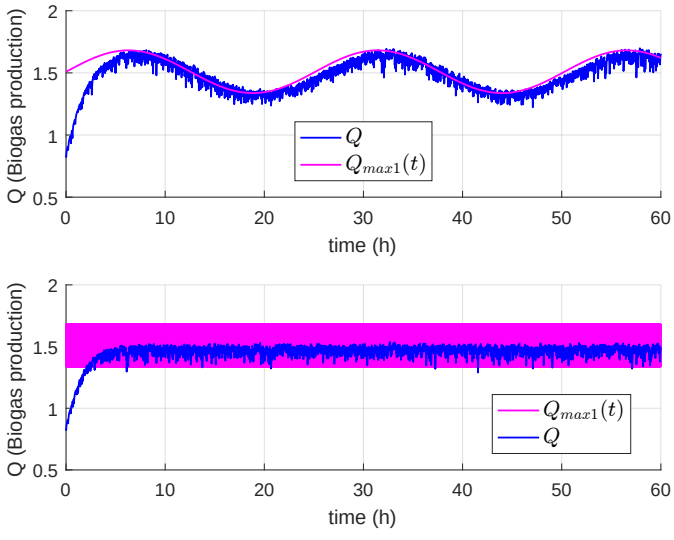

Figure 4.12: Monod reaction rate with CI_1, noise in measurements and time variant inlet-substrate-concentration $s_{in} = 1 + 0.1\sin(\omega t)$ (ω is 0.25 in the first plot and 200 in the second).

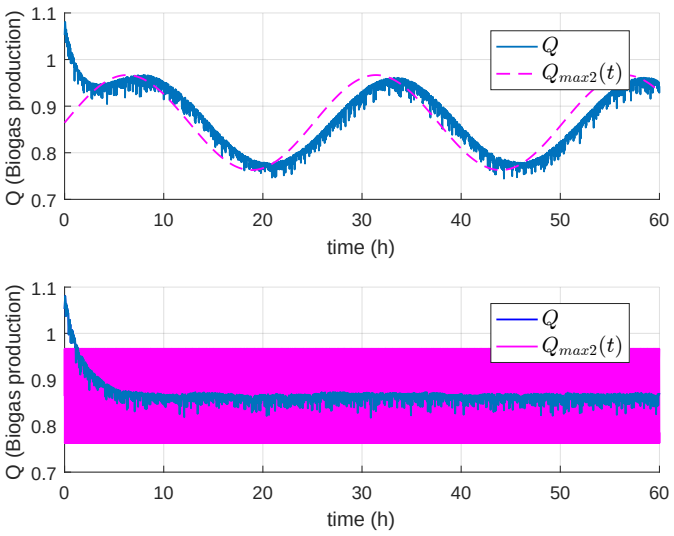

Figure 4.13: Haldane reaction rate with CI_2, noise in measurements and time variant inlet-substrate-concentration $s_{in} = 1 + 0.1\sin(\omega t)$ (ω is 0.25 in the first plot and 200 in the second).

Chapter 5

Conclusions

A bioreactor is a system, in which liquid waste can be transformed in biogas, i.e., energy is recovered from wastewater. Nevertheless, the amount of biogas is highly dependent on system parameters and reaction rate, which are usually unknown and difficult to determine.

One (obvious) control objective is the maximization of biogas production, which can be achieved by applying an extremum-seeking (ES) technique to the system. However, those controllers achieve the optimal operating point very slowly because they ignore system dynamics. Instead, in this work a control strategy based on the inherent system properties was designed and tested via simulations.

It was presented the analysis of a second order model for a Partially Fixed-Bed Reactor (PFBR), extending previos research made for a Continuous Stirred Tank Reactor (CSTR), i.e., one limit case in the analysis made is the CSTR (the biomass is suspended), and the other is the Fixed-Bed Reactor (FBR, where there is perfect biomass retention). Additionally, a positive invariant set for the system considering positive inputs was found.

A novel Extremum-Seeking strategy for optimizing bioreactors is presented, which uses only two input values, u_L and u_H, and is very robust because it is independent on the reaction rate model and system parameters. The controller was tested in continuous time, and system trajectories achieved convergence to a vicinity of the optimal operating point, independent of the reaction rate model, initial conditions and model parameters. Also, it was obvious that its performance was faster than traditional Extremum-Seeking strategies because the closed-loop time convergence was almost the same as with an optimal open-loop.

Additionally, closed loop performance was simulated considering a continuous system with a discrete controller, and noise in measurements. As in the previous case, it produced good results because system trajectories showed practical stability, i.e., biogas production was kept near its optimal value.

The controller design for the CSTR has the particularity that the only needed measurement

is the biogas production, i.e., the variable that is maximized is the only one needed.. On the other hand, for the PFBR it is necessary to measure a different output richer in information. It is important to mention that the algorithm is very simple and easy to implement.

The proposed strategy is therefore a very good option for optimizing these systems due to controller benefits. The authors hope to extend this methodology to higher order models (i.e. more realistic) for their future implementation.

Bibliography

Álvarez, J. and Franco, H. (2016). Geometric-dissipative control of exothermic continuous reactors. *IFAC-PapersOnLine*, 49(7):585–590. 13

Andrews, J. F. (1968). A mathematical model for the continuous culture of microorganisms utilizing inhibitory substrates. *Biotechnology and Bioengineering*, 10(6):707–723. 2, 19

Antonelli, R. and Astolfi, A. (2000). Nonlinear controllers design for robust stabilization of continuous biological reactors. In *Control Applications, 2000. Proceedings of the 2000 IEEE International Conference on*, pages 760–765. IEEE. 2, 19

Bacciotti, A. (2013). Stability of switched systems: an introduction. In *International Conference on Large-Scale Scientific Computing*, pages 74–80. Springer. 13, 14, 20, 26

Batstone, D. (2006). Mathematical modelling of anaerobic reactors treating domestic wastewater: Rational criteria for model use. *Reviews in Environmental Science and Biotechnology*, 5(1):57–71. 1

Blanchini, F. (1999). Set invariance in control. *Automatica*, 35(11):1747–1767. 13

Chang, J.-S., Lee, K.-S., and Lin, P.-J. (2002). Biohydrogen production with fixed-bed bioreactors. *International Journal of Hydrogen Energy*, 27(11-12):1167–1174. 2

Clarke, F. H., Ledyaev, Y. S., Sontag, E. D., and Subbotin, A. I. (1997). Asymptotic controllability implies feedback stabilization. *IEEE Transactions on Automatic Control*, 42(10):1394–1407. 25, 26

Cortes, J. (2008). Discontinuous dynamical systems. *IEEE control Systems*, 28(3). 25, 26

Dieulot, J.-Y. (2012). A productivity signal feedback controller for continuous bioreactors. *Journal of Process Control*, 22(7):1318–1324. 5

Guay, M., Dochain, D., and Perrier, M. (2004). Adaptive extremum seeking control of continuous stirred tank bioreactors with unknown growth kinetics. *Automatica*, 40(5):881–888. 5

Lara-Cisneros, G., Femat, R., and Dochain, D. (2014). An extremum seeking approach via variable-structure control for fed-batch bioreactors with uncertain growth rate. *Journal of Process Control*, 24(5):663–671. 3, 5

Lara-Cisneros, G., Femat, R., and Pérez, E. (2012). On dynamical behaviour of two-dimensional biological reactors. *International Journal of Systems Science*, 43(3):526–534. 19

Liberzon, D. (2012). *Switching in systems and control*. Springer Science & Business Media. 20, 26

Marcos, N., Guay, M., Dochain, D., and Zhang, T. (2004). Adaptive extremum-seeking control of a continuous stirred tank bioreactor with haldane's kinetics. *Journal of Process Control*, 14(3):317–328. 5

Moreno, J. A. (1999). Optimal time control of bioreactors for the wastewater treatment. *Optimal Control: Applications and Methods*, 20:145–164. 5

Schaum, A., Alvarez, J., and Lopez-Arenas, T. (2012). Saturated pi control of continuous bioreactors with haldane kinetics. *Chemical engineering science*, 68(1):520–529. 5, 10, 13, 19, 22

Sira-Ramírez, H. (1988). Differential geometric methods in variable-structure control. *International Journal of Control*, 48(4):1359–1390. 5

Wang, H.-H., Krstić, M., and Bastin, G. (1999). Optimizing bioreactors by extremum seeking. *Int. j. adapt. control signal process*, 13(651):669. 5, 40, 43, 44, 65, 66